Neuron

Article

# NDNF interneurons in layer 1 gain-modulate whole cortical columns according to an animal's behavioral state

## Graphical abstract

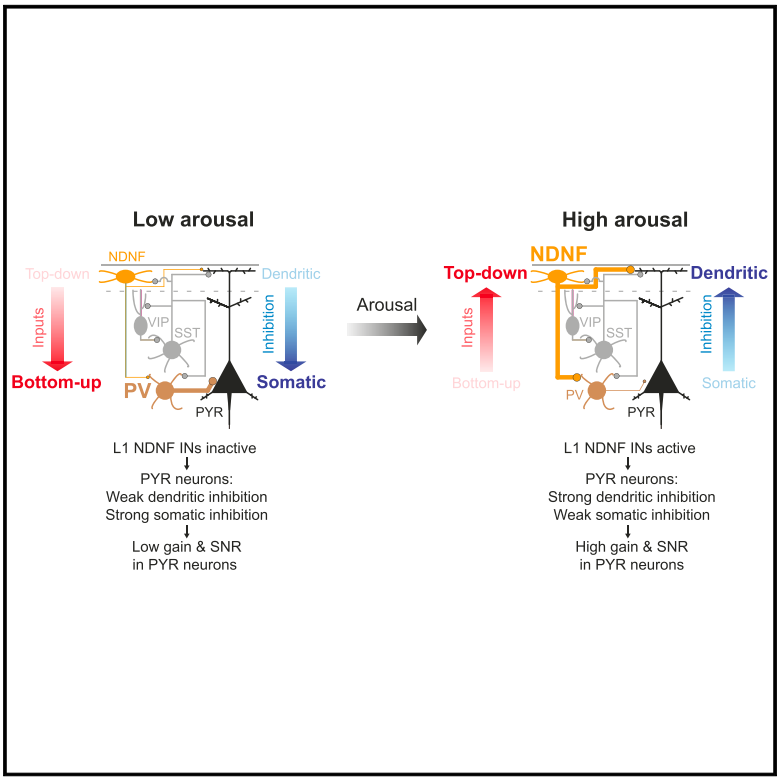


## Highlights

- Arousal strongly enhances the activity and sensory-evoked responses of L1 NDNF INs
- L1 NDNF INs gain-modulate local EXC neurons selectively during high-arousal states
- L1 NDNF INs inhibit the apical dendrites of EXC neurons and disinhibit their somata
- Active NDNF INs are evenly spread across L1 and can affect EXC neurons in all layers


## Authors

Katayun Cohen-Kashi Malina, Emmanouil Tsivourakis, Dahlia Kushinsky, ..., Adi Mizrahi, Ilan Lampl, Ivo Spiegel

## Correspondence

ivo.spiegel@weizmann.ac.il



## In brief

Cohen-Kashi Malina et al. show that visual cortex L1 NDNF INs are strongly driven by arousal. Active NDNF INs are evenly spread in L1 and gain-modulate local excitatory neurons in all cortical layers during high-arousal states by directly inhibiting their apical dendrites while disinhibiting their somata via *Parvalbumin*-expressing interneurons.


Cohen-Kashi Malina et al., 2021, Neuron *109*, 2150–2164
July 7, 2021 
https://doi.org/10.1016/j.neuron.2021.05.001

CellPress

CellPress

Neuron

Article

# NDNF interneurons in layer 1 gain-modulate whole cortical columns according to an animal's behavioral state

Katayun Cohen-Kashi Malina,[1] Emmanouil Tsivourakis,[1,3] Dahlia Kushinsky,[1,3] Daniella Apelblat,[1] Stav Shtiglitz,[1] Eran Zohar,[1] Michael Sokoletsky,[1] Gen-ichi Tasaka,[2] Adi Mizrahi,[2] Ilan Lampl,[1] and Ivo Spiegel[1,4,*]

[1]Department of Neurobiology, Weizmann Institute of Science, Rehovot, Israel

[2]Edmond & Lily Safra Center for Brain Sciences, Hebrew University of Jerusalem, Jerusalem, Israel

[3]These authors contributed equally

[4]Lead contact

*Correspondence: ivo.spiegel@weizmann.ac.il

https://doi.org/10.1016/j.neuron.2021.05.001

## SUMMARY

Processing of sensory information in neural circuits is modulated by an animal's behavioral state, but the underlying cellular mechanisms are not well understood. Focusing on the mouse visual cortex, here we analyze the role of GABAergic interneurons that are located in layer 1 and express *Ndnf* (L1 NDNF INs) in the state-dependent control over sensory processing. We find that the ongoing and sensory-evoked activity of L1 NDNF INs is strongly enhanced when an animal is aroused and that L1 NDNF INs gain-modulate local excitatory neurons selectively during high-arousal states by inhibiting their apical dendrites while disinhibiting their somata via *Parvalbumin*-expressing interneurons. Because active NDNF INs are evenly spread in L1 and can affect excitatory neurons across all cortical layers, this indicates that the state-dependent activation of L1 NDNF INs and the subsequent shift of inhibition in excitatory neurons toward their apical dendrites gain-modulate sensory processing in whole cortical columns.

## INTRODUCTION

The cortex's response to sensory stimuli is modulated by an animal's behavioral state, adjusting sensory perception to changing behavioral demands. The cellular mechanisms through which behavioral states modulate sensory responses in the cortex are still not well understood, but it is thought that layer 1 (L1; the cortex's uppermost layer) plays a prominent role in these mechanisms (Abs et al., 2018; Cauller, 1995; Ibrahim et al., 2016; Letzkus et al., 2011; Roth et al., 2016; Shlosberg et al., 2006). L1 is densely packed with the apical tuft dendrites of local excitatory neurons and with the axons of long-range projection neurons that convey sensory and behavioral state-dependent information from distal brain regions, including from other cortical areas (Ibrahim et al., 2016; Leinweber et al., 2017; Zhang et al., 2014), from thalamic nuclei (Cruz-Martín et al., 2014; Fang et al., 2020; Hu et al., 2019; Roth et al., 2016) and from neuromodulatory centers (Alitto and Dan, 2013). Thus, L1 is ideally suited for integrating sensory and state-dependent information, which together shape the activity of local excitatory neurons.

In addition to long-range axons and tuft dendrites, L1 also contains a sparse population of neurons, most of which belong to two subgroups of GABAergic interneurons (INs) (Abs et al., 2018; Jiang et al., 2013; Letzkus et al., 2011; Overstreet-Wadiche and McBain, 2015; Schuman et al., 2019; Tasic et al., 2016): neurogliaform cells (NGFCs) that express the neuron-derived neurotrophic factor (L1 NDNF INs) and that project laterally to the apical dendrites of local excitatory neurons through a dense axonal arbor (i.e., they innervate primarily L1 and layer 2/3 [L2/3]) and non-*Ndnf*-expressing INs that send a single axon downward into lower cortical layers (i.e., layer 4 [L4] to layer 6 [L6]). Considering their very different cellular properties, it seems likely that L1 IN subtypes exert rather different circuit functions; hence, subtype-specific approaches are required to unambiguously determine their function in the cortex. However, the lack of selective genetic access to either of these L1 IN subtypes has precluded assessing their role in sensory processing.

Here, we combine our recently established subtype-specific genetic tools and approaches with *in vivo* two-photon (2P) imaging, pupillometry, viral tracing, electrophysiology *ex vivo* and *in vivo*, chemogenetics, and optogenetics to investigate the role of L1 NDNF INs in the processing of visual information in the mouse primary visual cortex (V1). We find that L1 NDNF INs respond to visual stimuli in a unique manner compared with other types of cortical neurons and that their sensory-evoked responses are strongly enhanced when an animal is aroused. Consistent with this, we demonstrate that visual cortex L1 NDNF INs receive long-range inputs from many distal brain regions that can convey sensory-evoked and/or state-dependent information. Probing the downstream effects of L1 NDNF

 

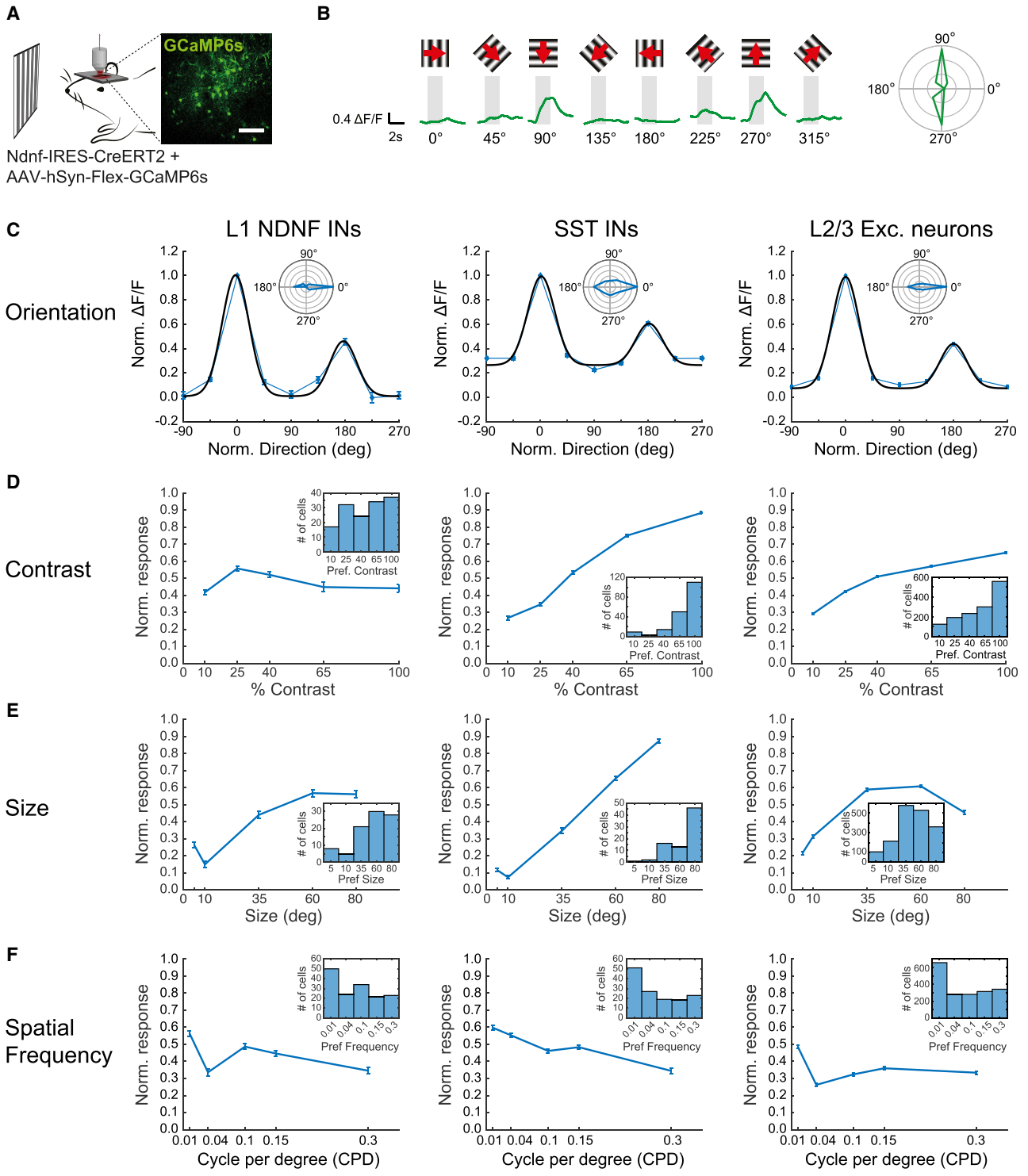


**Figure 1. Sensory-evoked responses of visual cortex L1 NDNF INs are cell-type specific**

(A) Left: setup for 2P imaging of GCaMP activity in L1 NDNF INs in V1 of awake mice. Right: field of view of GCaMP6s-expressing L1 NDNF INs in V1 (scale bar, 50 μm).

(B–E) Characterization of the visual response properties of L1 NDNF INs in V1 and comparison with those of SST INs and L2/3 excitatory neurons. (B and C) Orientation tuning. (B) Responses of a typical L1 NDNF IN to drifting gratings in different directions (left; gray area, visual stimulus) and corresponding polar plot (right). (C) Normalized population averages of all visually responsive L1 NDNF INs, SST INs, and L2/3 excitatory neurons at 100% contrast (138 L1 NDNF INs out of 362 imaged [38.12%], n = 8 mice; 99 SST INs out of 181 imaged [54.7%], n = 4 mice ; 803 L2/3 excitatory [Exc.] neurons out of 2,814 imaged [28.5%], n = 4 mice).

*(legend continued on next page)*

INs, we find that these neurons gain-modulate the activity and sensory-evoked responses of local excitatory neurons selectively during high-arousal states and improve their signal-to-noise ratio (SNR). L1 NDNF INs do so by conveying direct, long-lasting inhibition to excitatory neurons across all cortical layers and by concomitantly disinhibiting them via direct inhibition of fast-spiking (FS) INs that express *Parvalbumin* (PV INs). Because L1 NDNF INs target primarily the apical dendrites of cortical excitatory neurons, while PV INs specialize in targeting their somata, and because active NDNF INs are evenly spread across L1, our findings indicate that the behavioral state-dependent activation of L1 NDNF INs leads in local excitatory neurons to a relative shift of inhibition from the soma toward the apical dendrites and that this, in turn, enhances the stimulus-evoked responses in excitatory neurons across whole cortical columns and improves the SNR in these neurons.

## RESULTS

### Sensory-evoked responses of visual cortex L1 NDNF INs are cell-type specific

To study NDNF INs in the visual cortex, we first validated that they are concentrated in L1 in this region of the neocortex (Figure S1), similar to what we and others have reported for the auditory (AUD), somatosensory (SS), and prefrontal cortex (Abs et al., 2018; Anastasiades et al., 2021; Fan et al., 2020; Schuman et al., 2019). Using fluorescence *in situ* hybridization (FISH), we find that NDNF INs are indeed highly concentrated in L1 of the visual cortex, where they comprise about two-thirds (67.3%) of all GABAergic INs in L1 and express the same subtypes markers as in other cortical areas (including those markers found in NGFCs, e.g., *Reln*, *Npy*, and *Nos*; Cadwell et al., 2016).

Next, we assessed the visual response properties of L1 NDNF INs in the mouse V1 and compared them with those of somatostatin-expressing INs (SST INs), an IN subtype that also specializes in targeting the apical dendrites of local excitatory neurons (Tremblay et al., 2016), and with those of excitatory neurons in L2/3 of the cortex. To this end, we expressed the calcium indicator GCaMP6s in the respective neuronal subtype in V1 (i.e., in L1 NDNF INs, in SST INs, or in L2/3 excitatory neurons) via intracortical injections of adeno-associated viral (AAV) constructs and performed *in vivo* 2P imaging in awake head-fixed mice that were presented with drifting gratings at various directions, contrasts, stimulus sizes, and spatial frequencies, thereby respectively testing orientation tuning, contrast sensitivity, size selectivity, and visual acuity (i.e., spatial frequency) (Figure 1). These experiments revealed that 56.6% of the recorded L1 NDNF INs respond significantly to visual stimuli and that they are strongly orientation tuned (89% of all visually responsive L1 NDNF INs) (Figures 1B, 1C, and S2A). The responses of L1 NDNF INs are not strongly affected by the spatial frequency of the gratings presented to the mice, but they do exhibit a preference for low spatial frequency (Figure 1F; p = 1.6109e–05, Kruskal-Wallis one-way ANOVA). Similarly, increases in the size of the visual stimulus only moderately enhance the responses of L1 NDNF INs (i.e., their responses plateau before the maximal stimulus size; Figure 1E), consistent with the idea that L1 NDNF INs convey a certain degree of surround suppression (Fan et al., 2020). Furthermore, the visually evoked responses of L1 NDNF INs are, at the population level, only weakly affected by the contrast of the visual stimuli (Figure 1D): although the responses of individual L1 NDNF INs are contrast dependent, a similar percentage of L1 NDNF INs maximally respond at each contrast level, and thus, a similar number of L1 NDNF INs respond to visual inputs regardless of stimulus contrast (Figure 1D, inset). These response properties of L1 NDNF INs clearly differ from those of SST INs: SST INs are less orientation tuned than L1 NDNF INs (Figures 1C and S2; median global orientation selectivity index (gOSI) of SST INs = 0.305 versus median gOSI of L1 NDNF INs = 0.624, p = 9.56e–10, Kruskal-Wallis one-way ANOVA), but their responses directly scale with the contrast (Figure 1D) and the size (Figure 1E) of the visual stimulus. The response properties of L1 NDNF INs also differ from those of L2/3 excitatory neurons: while both types of neurons are strongly orientation tuned (Figures 1C and S2; median gOSI of L2/3 excitatory neurons = 0.683, p = 0.898, Kruskal-Wallis one-way ANOVA), the responses of L2/3 excitatory neurons are, unlike those of L1 NDNF INs, suppressed at large stimulus size (Figure 1E) and enhanced as the contrast of the stimulus increases (Figure 1D). Taken together, these experiments reveal that L1 NDNF INs in the visual cortex have cell-type-specific responses to visual stimuli (i.e., to bottom-up inputs) that clearly differ from the response properties of other types of neurons in V1: while L1 NDNF INs are strongly orientation tuned, their visually evoked responses remain, on the population level, relatively constant across varying levels of stimulus contrast and are only moderately enhanced upon increases in the size of the stimulus. The relatively subtle effects of the stimulus' contrast on the visually evoked responses of L1 NDNF INs are very different from those of SST INs and L2/3 excitatory neurons in which the extent of the visually evoked responses increases with the strength of the visual stimuli presented.

### Sensory-evoked responses of visual cortex L1 NDNF INs are strongly enhanced when an animal is aroused

L1 is thought to be a key site for the behavioral state-dependent regulation of the activity and sensory-evoked responses of cortical neurons. Thus, we next examined the extent to which the activity of L1 NDNF INs is affected by brain state and compared this with the state-dependent modulation of SST INs and L2/3 excitatory neurons. For this, we measured the relation between the spontaneous (i.e., ongoing) or visually evoked

(D) Contrast tuning. Normalized population averages of all visually responsive L1 NDNF INs, SST INs, and L2/3 excitatory neurons to visual stimuli at different contrast levels (144 L1 NDNF INs, n = 6 mice; 186 SST INs, n = 6 mice; 1,442 L2/3 Exc. neurons, n = 4 mice). (E) Size tuning. Normalized population averages of all visually responsive L1 NDNF INs, SST INs, and L2/3 excitatory neurons to visual stimuli of different sizes (in degrees) (92 L1 NDNF INs, n = 5 mice; 113 SST INs, n = 4 mice; 1,785 L2/3 Exc. neurons, n = 4 mice).
(F) Spatial frequency tuning. Normalized population averages of all visually responsive L1 NDNF INs, SST INs, and L2/3 excitatory neurons to gratings at different cycles per degree (cpd) (153 L1 NDNF INs, n = 5 mice; 138 SST INs, n = 4 mice; 1,873 L2/3 Exc. neurons, n = 4 mice).

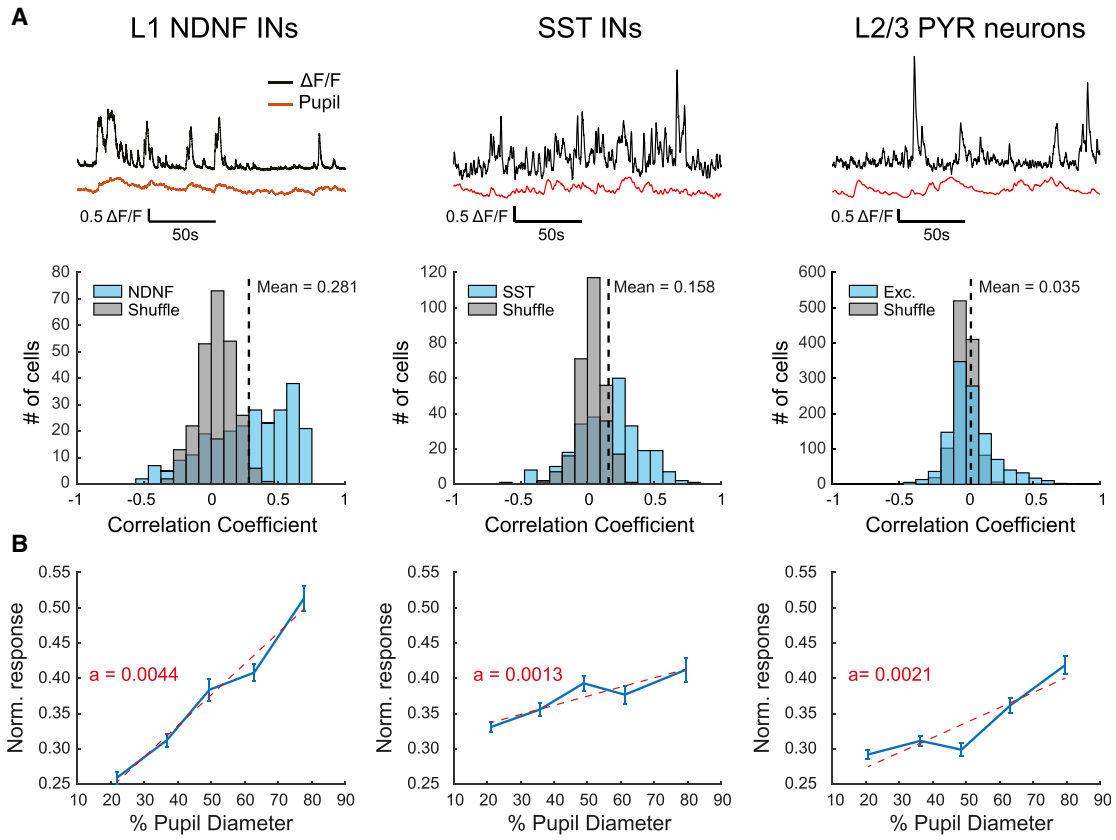


**Figure 2. Ongoing activity and visually evoked responses of L1 NDNF INs in V1 are strongly enhanced when an animal is aroused**

Pupillometry reveals that the activity of L1 NDNF INs in V1 strongly depends on brain state.

(A) Comparison of the ongoing activity of L1 NDNF INs, SST INs, and L2/3 excitatory neurons in V1 and of pupil diameter (i.e., arousal state). Top: example traces of the spontaneous GCaMP6s activity in the respective neuronal subtype (black) and of pupil diameter (ochre). Bottom: histogram of the correlation coefficients (Pearson correlation) of spontaneous GCaMP6s activity in the respective neuronal subtype with pupil diameter (L1 NDNF INs: dotted line = 0.2813 [population average of n = 250 L1 NDNF INs from seven mice]; gray, shuffled control; p = 1.52e–18, Wilcoxon signed-rank test; n = 287 SST INs from five mice, p = 4.6875e–14, Wilcoxon signed-rank test; n = 1,141 L2/3 Exc. neurons from four mice; p = 1.85e–06, Wilcoxon signed-rank test).

(B) Comparison of the evoked activity of L1 NDNF INs, SST INs, and L2/3 excitatory neurons in V1 and of pupil diameter (i.e., arousal state). The blue trace depicts the normalized average responses of each type of neuron to visual stimulation (at each cell's preferred direction) at the respective pupil diameter, the dotted red depicts the linear fit of the blue trace, and the red number indicates the slope of the dotted red line (L1 NDNF INs: n = 104 cells from seven mice, p = 0.0004, Kruskal-Wallis one-way ANOVA; SST INs: n = 149 cells from five mice, p = 0.565, Kruskal-Wallis one-way ANOVA; L2/3 Exc.: n = 813 cells from four mice, p = 1.65e–10, Kruskal-Wallis one-way ANOVA).

activity of the respective neuronal subtypes in V1 to the size of the animal's pupil, as pupillometry provides a robust indication of a mouse's arousal state (McGinley et al., 2015; Reimer et al., 2014; Vinck et al., 2015) (Figure 2). This analysis revealed that the spontaneous activity of L1 NDNF INs is strongly correlated with pupil diameter (mean correlation = 0.2813, p = 1.58e–18, Wilcoxon signed-rank test, shuffle pairs versus true pairs; Figure 2A) and that this correlation is higher in L1 NDNF INs than in SST INs (0.158, p = 0.0005, Kruskal-Wallis one-way ANOVA) or in L2/3 excitatory (0.035, p = 9.56e–10, Kruskal-Wallis one-way ANOVA). Further analysis of the spontaneous activity of L1 NDNF INs reveals that these neurons tend to be co-active (i.e., their spontaneous activity is correlated with each other) (Figures S2B and S2C); this correlated activity of L1 NDNF INs does not depend on their physical distance from each other (Figure S2D), but co-active L1 NDNF INs tend to be evenly spaced from each other (mean distance of 220.3 ± 1.5 μm between co-active NDNF INs in L1, similar to the radius of the their axonal arbor; Jiang et al., 2015; Schuman et al., 2019; Figure S2E). Consistent with the notion that the activity of L1 NDNF INs increases as the animal becomes more alert, we find that in anesthetized mice, only 42% of L1 NDNF INs are active (Figure S2F). When we then analyzed the state dependency of the evoked responses of L1 NDNF INs, we found that the amplitude of their responses strongly scales with pupil diameter (Figure 2B), indicating that L1 NDNF INs respond to the same visual stimulus much stronger when the animal is alert. Although a positive correlation between the strength of the visually evoked responses and the animal's arousal state is observed also in SST INs and L2/3 excitatory neurons (Figure 2B), this state-dependent modulation is much stronger in L1 NDNF INs. Thus, taken together, we conclude that the visually evoked

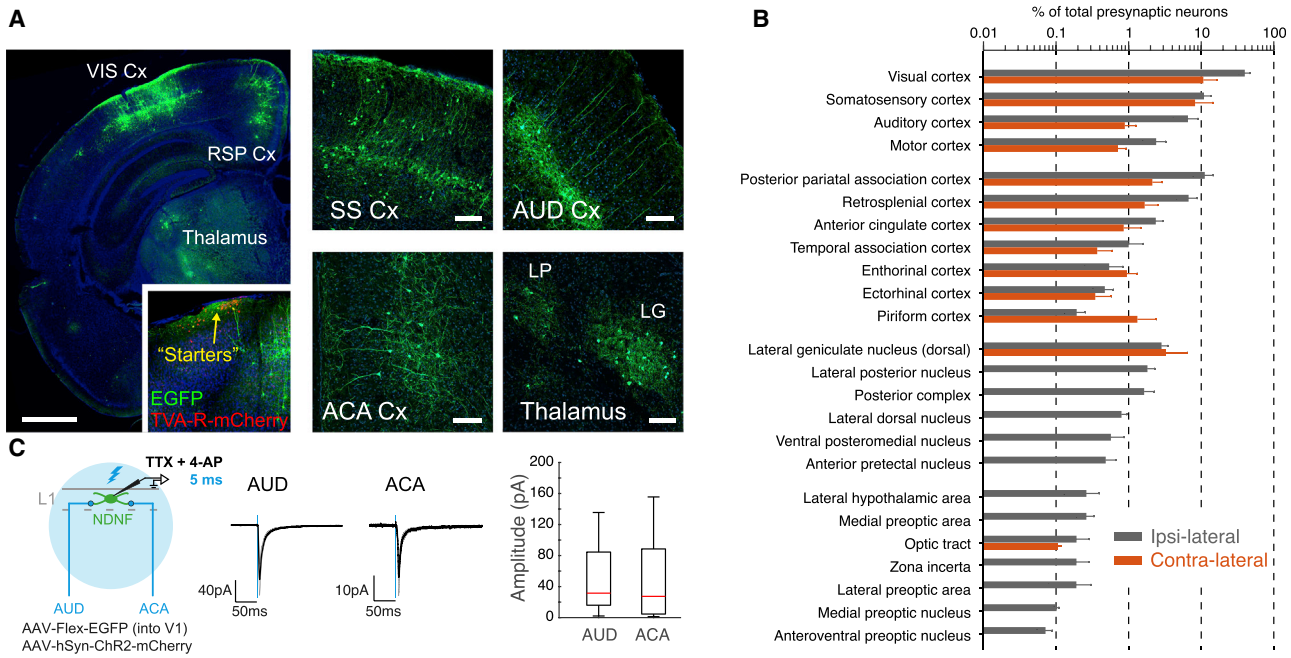


**Figure 3. Visual cortex L1 NDNF INs receive bottom-up and top-down synaptic inputs from distal brain areas**

(A and B) Rabies virus (RV)-based retrograde monosynaptic tracing reveals that L1 NDNF INs in the visual cortex receive long-range inputs from many distal brain regions that can convey bottom-up sensory and top-down behavioral state-dependent information. (A) Example images of Ndnf-IRES-CreERT2 mice injected into their visual cortex first with AAVs to drive expression of the rabies glycoprotein and the TVA receptor (fused to mCherry) selectively in L1 NDNF INs and then with a G protein-deficient RV that drives depression of EGFP and was pseudotyped with TVA. "Starter cells" are recognized by expression of TVA-R-mCherry and EGFP (see inset), while input cells express EGFP only (see examples from several distal brain regions: SS Cx, somatosensory cortex; AUD Cx, auditory cortex; ACA, anterior cingulate area cortex; LG, lateral geniculate complex; LP, lateral posterior nucleus) (scale bar in overview image, 1 mm; scale bars in brain regions, 100 μm). (B) Quantification of the EGFP-labeled presynaptic cells (n = 12,832 cells from five mice).

(C) Anterograde optogenetic mapping confirms the monosynaptic connectivity of distal brain regions to L1 NDNF INs in V1. AAVs for Cre-dependent expression of EGFP and for neuronal expression of ChR2 were respectively injected into V1 and either into the auditory cortex (AUD Cx) or anterior cingulate area (ACA) in the prefrontal cortex; photocurrents were measured in EGFP-labeled L1 NDNF INs in acute visual cortex slices in the presence of TTX and 4-AP (AUD, n = 19 cells; ACA, n = 19 cells). Left: scheme of experimental setup; middle: average of all traces (blue, optogenetic activation); right: summary of amplitudes in boxplot format.

responses of L1 NDNF INs are only weakly affected by the strength of visual stimulation (e.g., by stimulus contrast or size; Figures 1D and 1E) but are strongly tuned to an animal's behavioral state.

## Visual cortex L1 NDNF INs receive bottom-up and top-down synaptic inputs from distal brain areas

Having established that L1 NDNF INs in the visual cortex respond to visual inputs and that their activity is strongly modulated by an animal's arousal state, we next tested whether these neurons receive synaptic inputs from relevant brain areas, i.e., brain areas that can convey bottom-up visual information and/or top-down state-dependent or contextual information. To this end, we performed rabies virus-based retrograde monosynaptic tracing (Wickersham et al., 2007), with L1 NDNF INs in the visual cortex as starter cells. Having validated that the starter cells are indeed localized in L1 of the visual cortex (Figure 3A, inset), we prepared serial sections of the brains of the injected mice and quantified the amount of labeled (i.e., monosynaptically connected) neurons in each brain region (n = 12,832 neurons from five mice; Figure 3B). We find that L1 NDNF INs indeed receive direct inputs from brain regions that convey bottom-up visual inputs, including the dorsal lateral geniculate nucleus (dLG) in the thalamus. Similarly, we find that visual cortex L1 NDNF INs receive extensive inputs from many brain regions that can convey top-down information, including from other primary cortices (e.g., from the AUD, SS, and motor [MO] cortices), association cortices (e.g., from the retrosplenial [RSP] cortex and from the anterior cingulate area [ACA] in the prefrontal cortex), and higher-order thalamic nuclei (e.g., from the lateral posterior nucleus [LP] in the thalamus). In addition, we identify direct inputs from several hypothalamic nuclei, including the lateral hypothalamic area (LHA) and the medial preoptic area (MPA). Many of the inputs identified by our rabies tracing derive from both hemispheres, that is, from the hemispheres ipsi- and contralateral to the viral injection site, which is consistent with previous observations about the prominent role of L1 INs in interhemispheric inhibition (Palmer et al., 2012). To validate that the inputs identified by our rabies-tracing experiments are indeed monosynaptic and functional, we focused on the AUD and the prefrontal cortex and performed optogenetic input mapping to visual cortex L1 NDNF INs from these regions (Figure 3C). For this, we expressed the optogenetic activator ChR2 (Zhang et al., 2006) in the respective cortical area, labeled L1 NDNF INs in the visual cortex with GFP, and performed

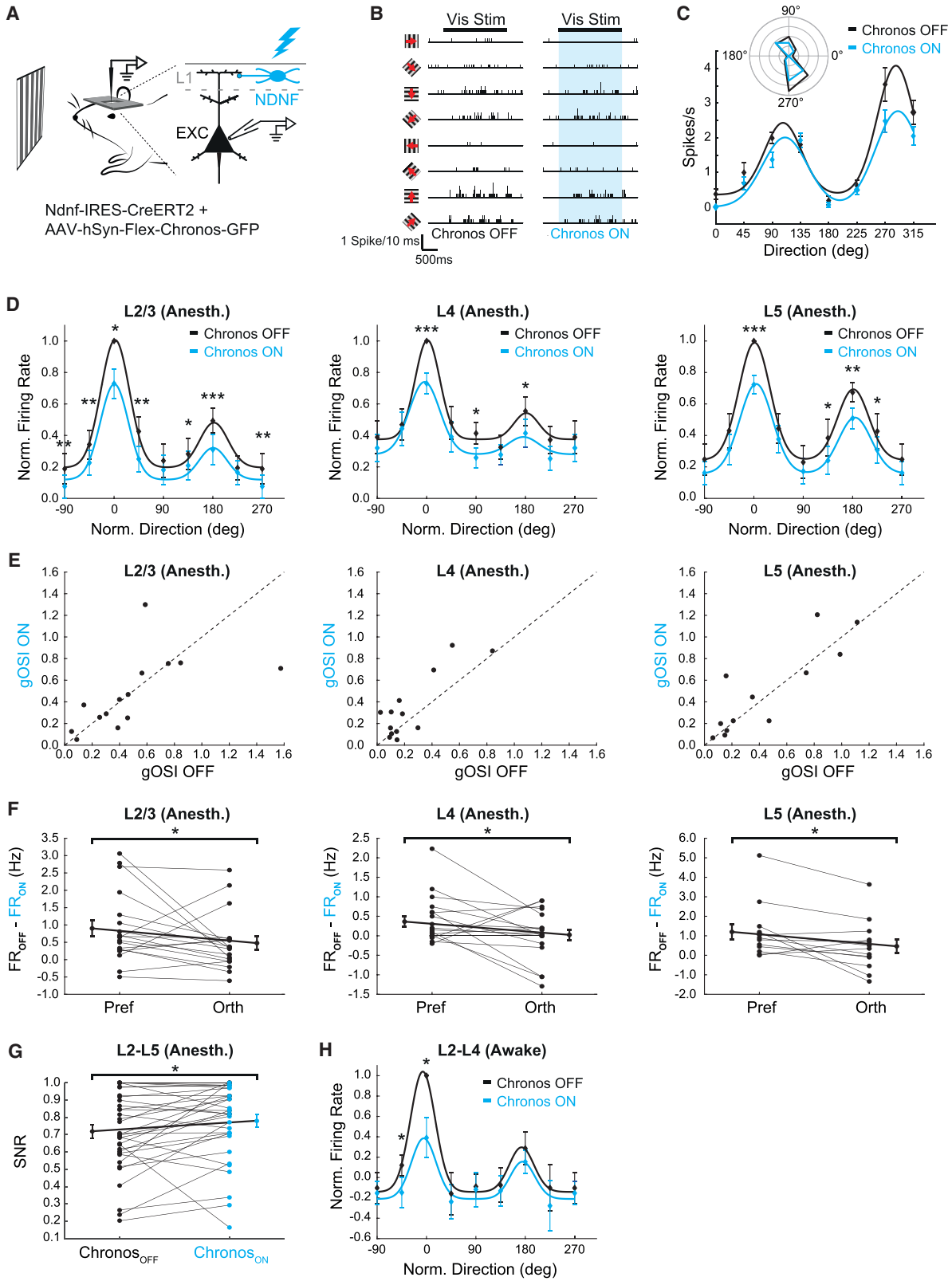


*(legend on next page)*

whole-cell voltage-clamp recordings from GFP-labeled cells in acute visual cortex slices in the presence of tetrodotoxin (TTX) and 4-AP while photo-activating the ChR2-expressing axons. This revealed that visual cortex L1 NDNF INs indeed receive direct monosynaptic inputs from the AUD and prefrontal cortex (Figure 3C). Taken together, these findings are consistent with and extend previous reports on the organization of long-range inputs to visual cortex L1 (Cruz-Martín et al., 2014; Ibrahim et al., 2016; Leinweber et al., 2017; Roth et al., 2016; Zhang et al., 2014) and demonstrate that L1 NDNF INs receive direct synaptic inputs from multiple brain areas that convey bottom-up visual information and top-down behavioral state-dependent information. Notably, the differences between our findings and previous reports on long-range inputs to other types of visual cortex neurons (Leinweber et al., 2017) are reminiscent of the cell-type-specific differences in long-range inputs observed in other cortical areas (Anastasiades et al., 2021; Naskar et al., 2021; Wall et al., 2016).

### L1 NDNF INs can gain-modulate the visually evoked responses of excitatory neurons in all cortical layers

Next, we assessed how the activity of L1 NDNF INs affects the visually evoked responses of local principal (i.e., excitatory) neurons. For this, we expressed the optogenetic activator Chronos-GFP (Klapoetke et al., 2014) (Figures S3A–S3E) in visual cortex L1 NDNF INs and performed loose patch-clamp recordings from excitatory neurons (see STAR Methods) across all cortical layers while displaying visual stimuli and activating L1 NDNF INs in interleaved trials by turning on a blue light-emitting diode (LED) (470 nm) during the time of stimulus presentation (Figure 4A). Recording in anesthetized mice, we find that optogenetic activation of L1 NDNF INs significantly reduces spontaneous firing (Figure S3G) and visually evoked responses in excitatory neurons across all layers (Figures 4B–4D) without affecting their gOSI (Figure 4E), their preferred orientation (Figure S3H), or their direction selectivity index (DSI; Figure S3I). The same effects were observed when we recorded in awake mice (Figure 4H). We then analyzed the type of inhibition that is conveyed by L1 NDNF INs onto excitatory neurons (i.e., subtractive or divisive; Carandini and Heeger, 1994; Isaacson and Scanziani, 2011; Wilson et al., 2012) by comparing the effects of optogenetic L1 NDNF IN activation on excitatory neuron responses in their preferred and orthogonal direction (Figure 4F). We find that the change in firing rate at the preferred orientation is significantly higher than the one in orthogonal orientation; together with the fact that we detect no change in gOSI (Figure 4E), this indicates that L1 NDNF INs provide divisive inhibition across all cortical layers. Considering the effects of L1 NDNF INs activation on spontaneous firing in excitatory neurons (Figure S3G), our findings also suggest that L1 NDNF INs improve the SNR in these neurons. Indeed, we find that optogenetic activation of L1 NDNF INs leads to a subtle but significant increase of the SNR in excitatory neurons (Figure 4G). Thus, our experiments demonstrate that L1 NDNF INs can gain-modulate the visually evoked responses of principal excitatory neurons across all cortical layers via divisive inhibition and improve their SNR.

### Direct inhibition by L1 NDNF INs reduces firing rates in excitatory neurons across all cortical layers for hundreds of milliseconds

We then set out to test how L1 NDNF INs exert their inhibitory effects on excitatory neurons across all cortical layers. We and others have shown in acute cortical slices that L1 NDNF INs can inhibit L2/3 excitatory neurons (Abs et al., 2018; Schuman et al., 2019), but a direct demonstration of inhibition (i.e., hyperpolarization) conveyed by L1 NDNF INs *in vivo* remained elusive. Thus, we recorded intracellularly from visual cortex excitatory neurons along the cortical column while optogenetically activating L1 NDNF INs. Recordings in anesthetized mice show that even short activation of L1 NDNF INs (50 ms) elicits a strong and long-lasting hyperpolarization (several hundred milliseconds) in excitatory neurons (Figures 5A and 5C), including in deep cortical layers (i.e., layer 5 [L5]). These effects are not due to anesthesia, as such long-lasting hyperpolarization was observed also in awake mice (Figure 5B). Accordingly, we find that the action potential firing rates of excitatory neurons across all cortical layers is reduced for at least 200 ms after the end of L1 NDNF IN activation (Figure 5D). To test whether this inhibition is the result of direct inputs from L1 NDNF INs to excitatory neurons, we expressed Chronos in L1 NDNF INs and performed whole-cell patch-clamp recordings from excitatory neurons in acute visual cortex slices in the presence of TTX and 4-AP while optogenetically activating L1 NDNF INs. Indeed, we find that

**Figure 4. L1 NDNF INs can gain-modulate the visually evoked responses of excitatory neurons in all cortical layers**

(A) Configuration for *in vivo* patch-clamp recordings from excitatory (EXC) neurons in V1 of awake or anesthetized mice while presenting visual stimuli and optogenetically activating L1 NDNF INs.

(B–E) Optogenetic activation of L1 NDNF INs reduces visually evoked responses of excitatory neurons in V1 across all layers but does not affect their orientation selectivity (B–E, anesthetized mice; F, awake mice). (B) Peristimulus time histogram (PSTH) of spike responses of a representative L2/3 excitatory neuron to drifting gratings without (black) and with (blue) optogenetic activation of L1 NDNF INs. (C) Fitted tuning curve and the average firing rate of the L2/3 example excitatory neuron in (B) in each direction (summarized in polar plot). (D) Average normalized responses of excitatory neurons across all layers when L1 NDNF INs are optogenetically activated (blue) or not (black). The responses of excitatory neurons in all layers are significantly reduced upon activation of L1 NDNF INs (L2/3, $n = 14$; L4, $n = 14$; L5, $n = 13$; $^{*}p < 0.05$, $^{**}p < 0.01$, and $^{***}p < 0.001$, Wilcoxon signed-rank test). (E) Global orientation selectivity index (gOSI) of excitatory neurons across all layers with (blue) and without (black) activation of L1 NDNF INs (L2/3, $p = 0.9515$; L4, $p = 0.7088$; L5, $p = 0.946$; Wilcoxon signed-rank test).

(F) L1 NDNF INs provide divisive inhibition across all cortical layers. The difference in the firing rates (FR) in V1 excitatory neurons without (OFF) or with (ON) optogenetic stimulation in L1 NDNF INs is significantly different between the preferred and orthogonal orientation across all layers (L2/3, $p = 0.0486$; L4, $p = 0.0437$; L5, $p = 0.0215$; Wilcoxon signed-rank test).

(G) Activation of L1 NDNF INs improves the signal-to-noise ratio (SNR) in L2–L5 excitatory neurons. The SNR was calculated as the difference between the neuron's evoked and spontaneous firing rate divided by the sum ($n = 34$ excitatory neurons, $p = 0.0273$, Wilcoxon signed-rank test).

(H) Average normalized responses of L2/3 and L4 excitatory neurons in V1 of awake mice when L1 NDNF INs are optogenetically activated (blue) or not (black) ($n = 9$, $^{*}p = 0.0273$, Wilcoxon signed-rank test).

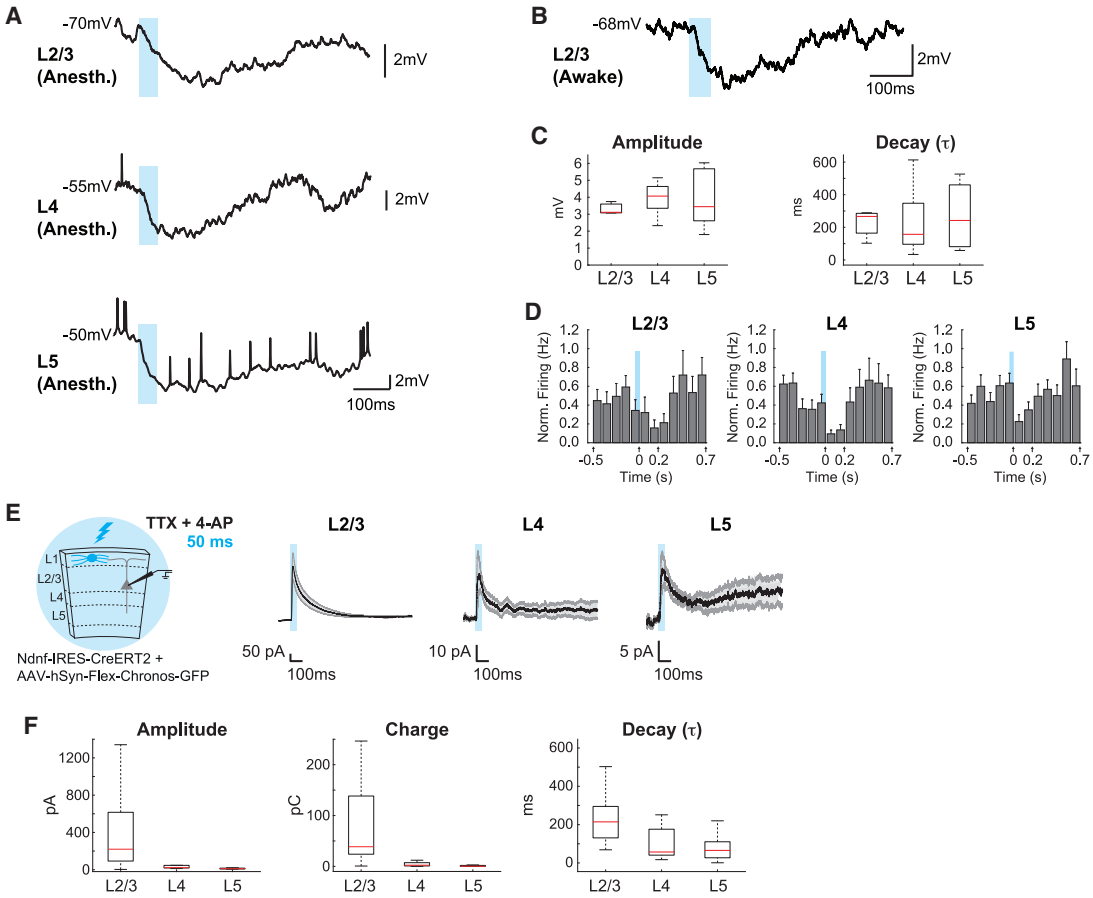


**Figure 5. Direct inhibition by L1 NDNF INs reduces firing rates in excitatory neurons across all cortical layers for hundreds of milliseconds**

(A–D) *In vivo* intracellular current-clamp recordings reveal that optogenetic activation of L1 NDNF INs leads to long-lasting hyperpolarization in V1 excitatory neurons across all layers. Example average traces of membrane potential recordings in anesthetized (A) and awake (B) mice. Blue shades mark the time of optogenetic activation of L1 NDNF INs. (C) Average amplitude and decay time in excitatory neurons in response to optogenetic activation of L1 NDNF INs in anesthetized mice (L2/3, n = 7; L4, n = 10; L5, n = 6; p = 0.2816 for amplitude, p = 0.7493 for decay, Kruskal-Wallis one-way ANOVA). (D) Average normalized peristimulus time histogram (PSTH; bin size = 100 ms; L2/3, n = 9; L4, n = 22; L5, n = 16).

(E and F) Whole-cell patch-clamp recordings in the presence of tetrodotoxin (TTX) and 4-AP in acute visual cortex slices reveal that L1 NDNF INs directly inhibit excitatory neurons in all layers of V1. (E) Left: experimental setup. Chronos-expressing L1 NDNF INs are optogenetically activated for 50 ms. Right: averaged inhibitory postsynaptic current (IPSC) traces of recorded excitatory neurons in each layer (L2/3, n = 17; L4, n = 10; L5, n = 20). (F) Average amplitude, charge transfer, and decay time in excitatory neurons upon optogenetic activation of L1 NDNF INs (amplitude, p = 7.42e–06; charge, p = 5.61e–06; decay, p = 0.0004; Kruskal-Wallis one-way ANOVA).

activation of L1 NDNF INs elicited inhibitory current in excitatory neurons across all cortical layers (Figures 5E and 5F), that this inhibition is direct and long-lasting (e.g., compared with inhibition from SST INs to excitatory INs; Abs et al., 2018), and that these inhibitory currents are mediated in part by $GABA_B$ receptors (Figures S4A and S4B). Together, these experiments demonstrate that L1 NDNF INs can inhibit excitatory neurons across all cortical layers via direct inhibitory currents, thereby leading to a long-lasting reduction in their firing rates.

## L1 NDNF INs enhance visually evoked responses and improve SNR in excitatory neurons in a state-dependent manner

Having established that L1 NDNF INs respond to visual stimuli in a state-dependent manner and that their exogenous optogenetic activation can modulate the visually evoked responses of excitatory neurons via direct long-lasting inhibition, we next tested whether the endogenous activity of L1 NDNF INs indeed modulates the visually evoked responses of excitatory neurons in a manner that depends on the animal's behavioral state. To this end, we measured the activity of visual cortex L2/3 excitatory neurons in awake mice via 2P GCaMP imaging prior to and after chemogenetic inhibition of L1 NDNF INs and while assessing the animal's arousal state via pupillometry (Figure 6A). Importantly, we first confirmed (1) that the chemogenetic inhibition of L1 NDNF INs indeed abolishes optogenetically activated inhibitory currents from these neurons to visual cortex L2/3 excitatory neurons (Figures S5A–S5C) and (2) that the chemogenetic inhibition of L1 NDNF INs does not alter the animal's arousal state (Figure S5D). When we then tested whether the inhibition of L1

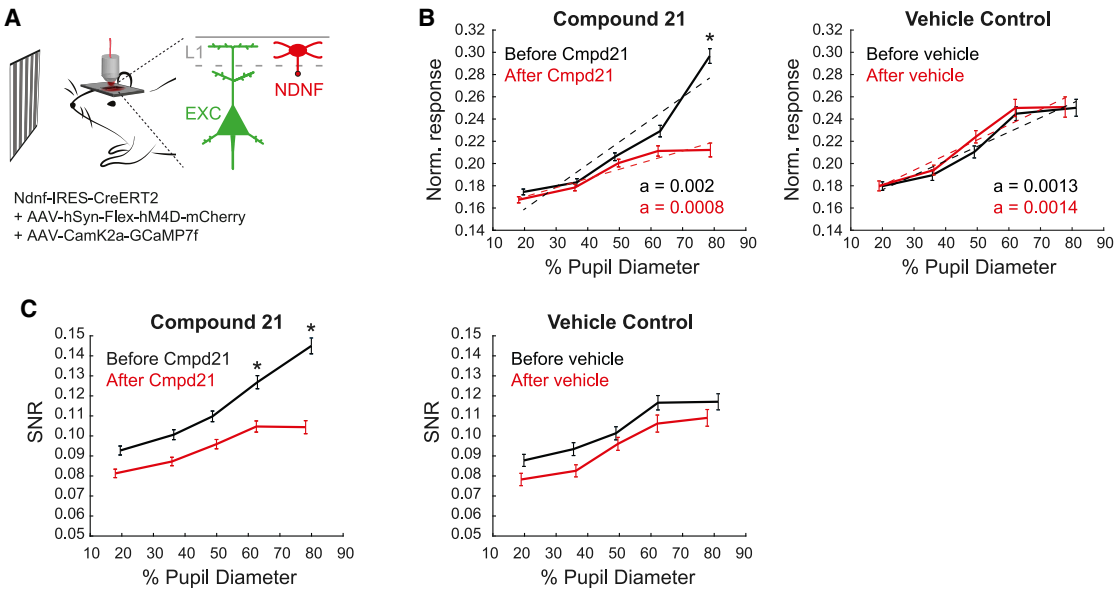


**Figure 6. L1 NDNF INs modulate SNR in excitatory neurons in a state-dependent manner**

(A) Configuration for *in vivo* two-photon imaging of GCaMP-activity of L2/3 excitatory (EXC) neurons in V1 of awake mice while presenting visual stimuli before and after chemogenetic inactivation of L1 NDNF INs that express the inhibitory DREADD hM4D(Gi)-mCherry; pupillometry was conducted throughout the whole experiment to assess arousal state.

(B) L1 NDNF INs control the visually evoked responses in L2/3 excitatory neurons in a behavioral state-dependent manner. The black and red traces depict the normalized average responses of the same neurons to visual stimulation (at each cell's preferred direction) at the respective pupil diameter before and after intraperitoneal (i.p.) injection of either compound 21 (i.e., agonist of hM4D; left plot) or of vehicle control (right plot); the dotted lines depict the linear fit of the respective trace, and a indicates the slope of the dotted respective line. A significant difference in visually evoked responses is observed upon injection of compound 21 only at high arousal, while no difference is observed upon injection of vehicle control ($p = 0.0001$, Wilcoxon rank-sum test).

(C) Inhibition of L1 NDNF INs reduces SNR in excitatory neurons selectively in high-arousal states. SNR was calculated for each L2/3 excitatory neuron at its preferred direction before and after inhibition of L1 NDNF INs (SNR was calculated as the difference between the evoked and inter-stimulus time interval dF/F divided by the sum of them). A significant difference in SNR is observed upon injection of compound 21 only at high-arousal states, while no difference is observed upon injection of vehicle control ($p = 0.0243$ and $p = 0.0053$ at ~65% and 80% pupil diameter, respectively).

NDNF INs affects the visually evoked responses of L2/3 excitatory neurons in a state-dependent manner, we found a significant reduction in the responses of the excitatory neurons only when the animals are aroused but not in low-arousal states ($p = 9e{-}05$, Wilcoxon rank-sum test). This reduction in the state-dependent increase of visually evoked response in L2/3 excitatory neurons was not observed when the animals were injected with the inert vehicle (DMSO) instead of the active chemogenetic compound 21.

Next, we tested how the SNR of L2/3 excitatory neurons is affected by the arousal state of the animal and whether L1 NDNF INs play a role in such modulation, as predicted by our finding in anesthetized mice (Figure 4G). Consistent with previous work (Vinck et al., 2015), we find that the SNR of L2/3 excitatory neurons improves as the animal becomes more alert (Figure 6C; $p = 0.0014$, low versus high pupil diameter, Kruskal-Wallis one-way ANOVA) and that the inhibition of L1 NDNF INs affects the SNR in a state-dependent manner, that is, that upon inhibition of L1 NDNF INs, the SNR of L2/3 excitatory neurons decreases significantly only in high-arousal states. Thus, we conclude that the endogenous activation of L1 NDNF INs at high-arousal states improves the SNR in L2/3 excitatory neurons.

## L1 NDNF INs can disinhibit excitatory neurons by inhibiting PV INs

The state-dependent modulation of the evoked responses and improvement of the SNR in L2/3 excitatory neurons by L1 NDNF INs (Figures 6B and 6C) likely involves not only direct inhibition as suggested by our optogenetic experiments in anesthetized mice (Figure 4) but also involves a disinhibitory mechanism: if indeed L1 NDNF INs inhibit inhibitory neurons that themselves inhibit excitatory neurons, this could explain why the chemogenetic inhibition of L1 NDNF INs in awake mice leads to a state-dependent reduction in the activity of L2/3 excitatory neurons rather than to an increase, as would have been expected if L1 NDNF INs would have provided only direct inhibition onto these excitatory neurons. We and others have previously shown that L1 INs can inhibit GABAergic INs in lower cortical layers (Abs et al., 2018; Jiang et al., 2013, 2015; Letzkus et al., 2011), but the identity of the INs targeted by L1 NDNF INs remains unknown. Thus, as INs that express either *Parvalbumin* (i.e., PV INs) or *Somatostatin* (i.e., SST INs) are the two major IN subtypes that directly inhibit excitatory neurons in the cortex—they respectively target either the soma or the apical dendrites of cortical excitatory neurons (Tremblay et al., 2016)—we tested whether L1 NDNF INs directly inhibit either of these

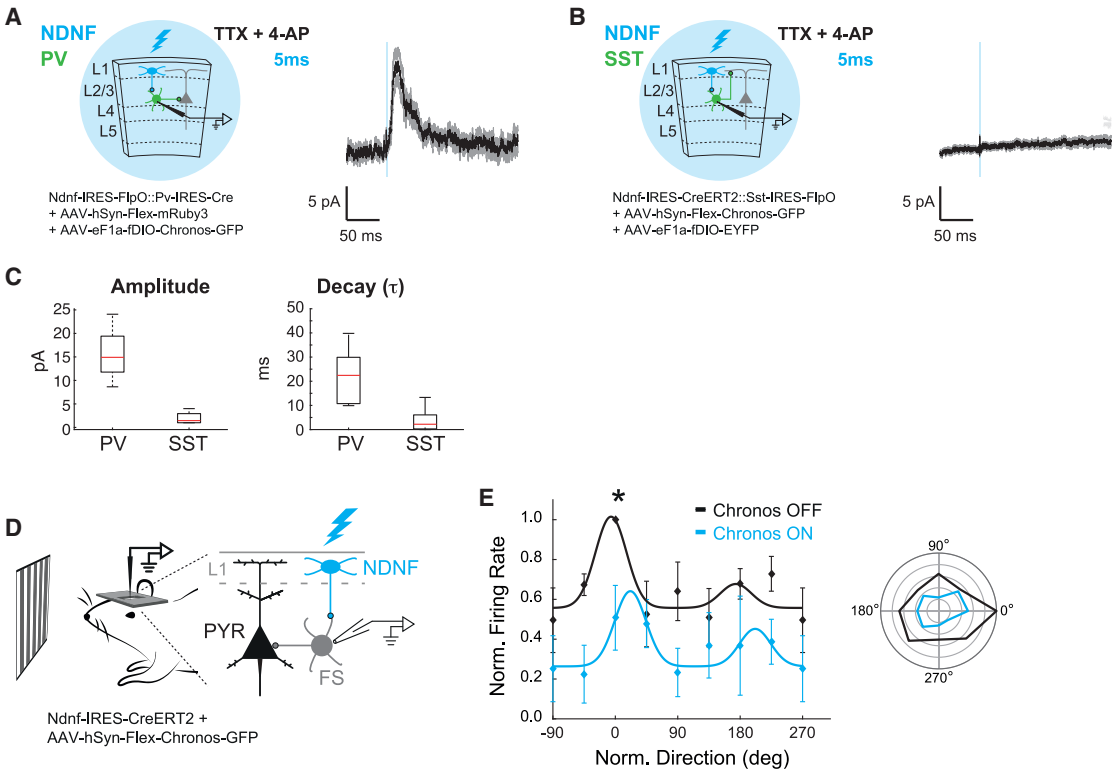


**Figure 7. L1 NDNF INs can disinhibit excitatory neurons by inhibiting PV INs**

(A–C) Visual cortex L1 NDNF INs can directly inhibit PV INs, but not SST INs. (A and B) Chronos-GFP was expressed in visual cortex L1 NDNF INs, while PV INs and SST INs were labeled respectively either with mRuby or EYFP; optogenetic recordings in acute visual cortex slices in the presence of TTX and 4-AP reveal that stimulation of L1 NDNF INs elicits photocurrents in PV INs (in 6 of 16 recorded cells) but not in SST INs (in 0 of 17 recorded cells) (shown are averaged IPSC traces of the 6 responsive PV INs and of the 17 non-responsive SST INs). (C) Summary of the experiments in (A) and (B).

(D and E) Activation of L1 NDNF INs reduces the visually evoked responses of fast-spiking neurons in V1. (D) Configuration for *in vivo* patch-clamp recordings from fast-spiking (FS) neurons in V1 of anesthetized mice while presenting visual stimuli and optogenetically activating L1 NDNF INs. (E) Average normalized responses of FS neurons across different stimulus directions when L1 NDNF INs are optogenetically activated (blue) or not (black). The responses of FS neurons are significantly reduced in their preferred direction upon activation of L1 NDNF INs (n = 6, p = 0.0313, Wilcoxon signed-rank test; summarized in polar plot).

two subtypes. To this end, we expressed Chronos in L1 NDNF INs while labeling either PV INs or SST INs with a fluorescent protein, prepared acute visual cortex slices, and performed whole-cell patch-clamp recordings from the fluorescently labeled neurons in the presence of TTX and 4-AP while optogenetically activating the Chronos-expressing L1 NDNF INs. This revealed that L1 NDNF INs directly inhibit PV INs, but not SST INs (Figures 7A and 7C). To test whether L1 NDNF INs can inhibit PV INs also *in vivo*, we then recorded in loose-patch configuration from electrophysiologically identified FS INs in the visual cortex of anesthetized mice expressing Chronos in L1 NDNF INs while displaying visual stimuli and optogenetically activating L1 NDNF INs in interleaved trials during the stimulus presentation (Figure 7D). This revealed that the activation of L1 NDNF INs indeed reduces the visually evoked responses of FS INs (Figure 7D). Thus, as FS INs in the cortex are largely PV positive (Fishell and Kepecs, 2020; Tremblay et al., 2016), we conclude that L1 NDNF INs inhibit FS PV INs in the visual cortex *in vivo* and that this, in turn, can disinhibit the soma of local excitatory neurons.

## DISCUSSION

We and others have recently identified several types of genetically defined GABAergic INs in L1 (Abs et al., 2018; Schuman et al., 2019; Tasic et al., 2016), but their roles in information processing in cortical circuits have remained largely unknown. Focusing on L1 NDNF INs in the adult visual cortex, here we demonstrate (1) that these INs respond to visual stimuli in a cell-type-specific manner, as they are orientation tuned, are modulated only moderately by stimulus size and spatial frequency, and are driven rather uniformly across varying stimulus contrasts; (2) that their spontaneous activity and sensory-evoked responses are strongly enhanced when an animal is aroused; (3) that they receive long-range inputs from multiple brain regions that can convey sensory-driven bottom-up inputs and behavioral state-dependent top-down inputs; (4) that they can provide direct, long-lasting divisive inhibition to local excitatory neurons across all cortical layers, probably via their apical dendrites; (5) that in parallel to this long-lasting dendritic inhibition, L1 NDNF INs disinhibit the somata of visual cortex

excitatory neurons by directly inhibiting FS PV INs; and (6) that the net effect of this state-dependent dendritic inhibition and somatic disinhibition by L1 NDNF INs is a gain modulation in the visually evoked responses of excitatory neurons across all layers of V1 and an increase in the SNR of their visually evoked responses. These findings are consistent with previous observations that long-range inputs to L1 from higher-order thalamic nuclei (Fang et al., 2020), other cortical areas (Ibrahim et al., 2016; Zhang et al., 2014), and neuromodulatory centers (Pinto et al., 2013) affect visual processing. Similarly, our findings are consistent with reports that L1 INs in mouse SS cortex are driven by contextual inputs (Brombas et al., 2014; Fan et al., 2020), that INs in L1 can inhibit INs in lower cortical layers (Abs et al., 2018; Jiang et al., 2013; Letzkus et al., 2011), and that pyramidal excitatory neurons across all layers of V1 extend their dendrites into L1 (Olsen et al., 2012; Scala et al., 2019).

Previous studies in the visual cortex have demonstrated that genetically defined IN subtypes (e.g., INs that express *Parvalbumin*, *Somatostatin*, or the *Vasoactive Intestinal Peptide* [PV, SST, or VIP INs, respectively]) respond to visual stimuli and modulate the visually evoked responses of local excitatory neurons in subtype-specific manners (Atallah et al., 2012; Ayzenshtat et al., 2016; Lee et al., 2012; Wilson et al., 2012) and that their activity depends on an animal's behavioral state (Dipoppa et al., 2018; Pakan et al., 2016). However, the lack of selective genetic access has precluded such subtype-specific analyses for L1 INs, and manipulating L1 INs with non-specific approaches yielded conflicting results (see, e.g., Ibrahim et al., 2016; Fang et al., 2020); thus, our analyses of L1 NDNF IN function address this gap in knowledge. Our findings indicate that the visually evoked responses of L1 NDNF INs and the state dependency of these responses are very different from those of other types of visual cortex neurons. Particularly when compared with SST INs (another type of IN that preferentially targets the apical dendrites of local excitatory neurons), it is clear that the response properties of L1 NDNF INs are cell-type specific: consistent with previous observations (Adesnik et al., 2012; Millman et al., 2020), we find that increasingly stronger contrast or larger size of the visual stimulus elicits in SST INs increasingly stronger responses while an animal's arousal state only moderately affects the responses of these INs; this is in stark contrast to L1 NDNF INs whose visually evoked responses are strongly enhanced as an animal becomes more aroused but respond rather uniformly to varying levels of contrast and are less affected by the size of the visual stimulus than SST INs (notably, pupil dilation per se does not enhance visually evoked responses in V1; Neske et al., 2019). As we and others have previously demonstrated in *ex vivo* experiments that SST INs can directly inhibit L1 NDNF INs (Abs et al., 2018; Jiang et al., 2015), one possibility is that these two IN subtypes act *in vivo* in mutually exclusive manners, for example, that SST INs provide inhibition to the apical dendrites of local excitatory neurons upon strong visual stimulation (i.e., bottom-up input) while L1 NDNF INs inhibit these dendrites when an animal is aroused (i.e., top-down input). However, considering that the activity of SST INs is also state dependent to some degree, a mutually exclusive "either-or" mechanism seems unlikely. Furthermore, as SST INs inhibit tuft dendrites via rapid synaptic inhibition (Tremblay et al., 2016) while L1 NDNF INs convey long-lasting inhibition via localized bulk release of GABA (i.e., "$GABA_{slow}$"; Abs et al., 2018; Schuman et al., 2019; Tamás et al., 2003), it seems more likely that the inhibition conveyed by these two IN subtypes to specific dendritic branches serves different biological purposes and thereby rather complement each other than compete with each other. Thus, future experiments will have to clarify how L1 NDNF INs and SST INs affect each other's activity in the visual cortex of awake mice and how this, in turn, affects inhibition and visually evoked responses in specific branches of excitatory neuron tuft dendrites. These future experiments will also have to include analyses of the potential interactions between L1 NDNF INs and VIP INs: similar to L1 NDNF INs, also VIP INs are activated in a behavioral state-dependent manner (e.g., during locomotion; Ferguson and Cardin, 2020; Fu et al., 2014), and as VIP INs control the activity of SST INs (Pfeffer et al., 2013), it will be important to test whether and how L1 NDNF INs and VIP INs interact with each other during different behavioral states to modulate the activity and sensory-evoked responses of local excitatory neurons and their apical dendrites.

Our results indicate that L1 NDNF INs, similar to other IN subtypes, gain-modulate the sensory-evoked responses of neighboring excitatory neurons via divisive inhibition (Atallah et al., 2012; Isaacson and Scanziani, 2011; Lee et al., 2012; Wilson et al., 2012; but see also Phillips and Hasenstaub, 2016) and that they improve the SNR in excitatory neurons. However, while other IN subtypes gain-modulate the flow of information in specific cortical subcircuits and only over short timescales (i.e., several milliseconds) (e.g., VIP INs; Fu et al., 2014; Walker et al., 2016), L1 NDNF INs provide gain modulation across all cortical layers and over very long timescales (hundreds of milliseconds). L1 NDNF INs seem to do so by eliciting inhibition and disinhibition at the same time, a mechanism that is very different from other IN subtypes that gain-modulate principal excitatory neurons either via direct inhibition (e.g., PV INs; Atallah et al., 2012) or disinhibition (e.g., VIP INs; Fu et al., 2014). Notably, the electrophysiology/optogenetics experiments (Figures 4 and 5) and imaging/chemogenetics experiments (Figure 6) that reveal this dual-action mechanism complement rather than contradict each other. Our electrophysiological recordings in anesthetized mice allowed us to analyze the effects of L1 NDNF IN activation on excitatory neuron activity across all cortical layers (Figures 4 and 5) which is currently not possible with conventional 2P-based GCaMP imaging. As the recordings in these gain-of-function experiments were made in cell-attached mode at the soma of excitatory neurons, they necessitated a relatively strong optogenetic activation of L1 NDNF INs, which led to a net inhibition of the recorded neurons; however, as revealed by our chemogenetic loss-of-function imaging experiments in awake animals (Figure 6), this inhibition masked the "true" somatic disinhibition provided by L1 NDNF INs via PV INs selectively during high-arousal states. Thus, the combination of electrophysiological/optogenetic approaches in anesthetized animals and of imaging/chemogenetic approaches in awake animals was very useful for analyzing the *in vivo* function of L1 NDNF INs and for dissecting the underlying cellular mechanisms.

Our findings indicate that at times of high arousal, the top-down-mediated activation of L1 NDNF INs leads to a relative

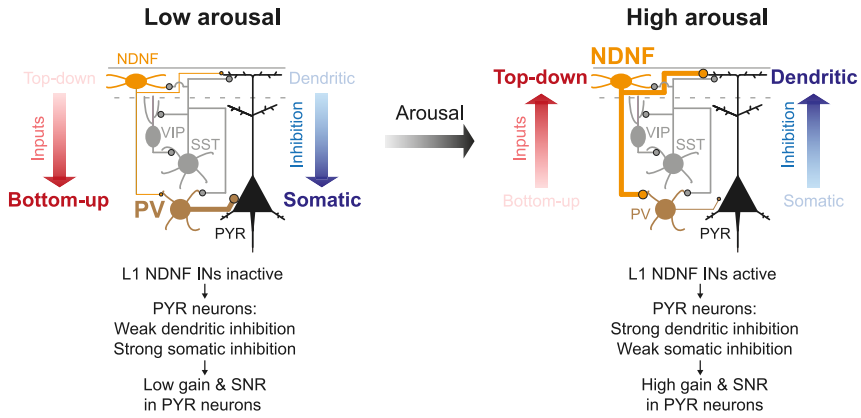


**Figure 8. State-dependent activation of L1 NDNF INs shifts inhibition in cortical excitatory neurons from the soma to the apical dendrites to gain-modulate the sensory-evoked responses of whole cortical columns and increase their SNR**

Behavioral state-dependent activation of L1 NDNF INs leads to direct inhibition of the apical dendrites in local excitatory neurons (PYR neurons) across all cortical layers and to the disinhibition of their somata via activation of *Parvalbumin*-expressing interneurons (PV INs). In turn, this leads to state-dependent gain modulation of sensory-evoked responses in excitatory neurons across all cortical layers and to higher SNR in these neurons. Thus, as L1 NDNF INs are co-active and evenly spread across L1, thereby covering the whole cortical surface, L1 NDNF INs can gain-modulate the sensory-evoked responses of large swaths of the cortex (i.e., of whole cortical columns) according to an animal's behavioral state.

shift of inhibition from the soma toward the apical dendrites in excitatory neurons across all cortical layers and that this improves the SNR upon bottom-up sensory stimulation (Figure 8). As (1) L1 NDNF INs extend their axonal arbors in L1 over large horizontal distances (the radius of their axonal arbor extends laterally 150–300 μm; Jiang et al., 2015; Schuman et al., 2019), (2) the (spontaneous) activity of L1 NDNF INs tends to be correlated (Figure S1C), (3) co-active L1 NDNF INs are distributed rather evenly in L1 and have a mean distance of ~220 μm from each other (Figures S1D and S1E), and (4) a similar number of L1 NDNF INs is active regardless of stimulus contrast, this also suggests that the state-dependent activation of L1 NDNF INs affects sensory-evoked responses in large swaths of a given cortical area. Thus, as L1 NDNF INs have now been described in multiple cortical areas (including visual [this study and Tasic et al., 2016], AUD [Abs et al., 2018], SS [Fan et al., 2020; Schuman et al., 2019], and prefrontal [Abs et al., 2018; Anastasiades et al., 2021] cortex), we propose that L1 NDNF INs are part of a canonical circuit motif through which long-range inputs to L1 can powerfully gain-modulate the responses of local excitatory neurons across all cortical layers and improve the SNR of whole local cortical circuits according an animal's behavioral state (Larkum et al., 2004) by shifting the relative amount of inhibition within excitatory neuron from their somata to their dendritic tufts. Future experiments will have to test this idea, for example by using novel molecular tools that allow direct imaging of GABAergic inhibition (Marvin et al., 2019). Similarly, future efforts will have to clarify (1) additional behavioral conditions under which L1 NDNF INs and their long-range inputs are recruited to gain-modulate the sensory-evoked responses of visual cortex principal neurons and (2) how L1 NDNF INs function in other cortical areas, particularly those areas where sensory gain seems to be modulated differently (e.g., AUD cortex; Abs et al., 2018; Schneider et al., 2014).

In addition to controlling sensory processing, the level of inhibition in tuft dendrites powerfully controls the experience-dependent plasticity of dendritic synapses (Bar-Ilan et al., 2013) and is thought to play a key role, for example, during learning (Abs et al., 2018; Adler et al., 2019; Chen et al., 2015; Lovett-Barron et al., 2014). Thus, a potential implication of our findings is that by inducing a long-lasting relative shift in inhibition toward the apical dendrites of excitatory neurons, L1 NDNF INs might generate the conditions for state-dependent stimulus-selective dendritic plasticity: on one side, the inhibitory activity of L1 NDNF INs slightly reduces the membrane potential ($V_m$) in the apical dendrites for 200–300 ms and thereby makes it harder for plasticity to occur in dendritic synapses (i.e., selectivity is increased), but at the same time, the somatic disinhibition facilitates the generation of back-propagating action potentials upon sensory (i.e., bottom-up) input to the soma, which in turn may drive plasticity at synapses in the apical dendrites in response to these specific stimuli. Thus, an exciting possibility is that L1 NDNF INs not only improve the SNR of the sensory-evoked responses of the excitatory neurons in whole cortical columns when an animal is aroused but that they also enable the animal's long-term adaptation (i.e., "learning") to these sensory stimuli by facilitating selective synaptic plasticity in the excitatory neurons' apical dendrites. L1 NDNF INs therefore might be a central part in the cellular mechanisms that link between behavioral state-dependent changes in perception and state-dependent learning.

## STAR★METHODS

Detailed methods are provided in the online version of this paper and include the following:

- KEY RESOURCES TABLE
- RESOURCE AVAILABILITY
  - Lead contact
  - Materials availability
  - Data and code availability
- EXPERIMENTAL MODEL AND SUBJECT DETAILS
  - Mice
- METHOD DETAILS
  - Fluorescent *in situ* hybridization (FISH)

- AAV stocks
- Viral injections and cranial window implantations
- Preparation of animals for *in vivo* electrophysiological recordings
- *In vivo* patch-clamp electrophysiology in the cortex
- Visual stimulation
- Optogenetic stimulation
- Chemogenetic silencing of L1 NDNF INs
- Patch-clamp electrophysiology in acute visual cortex slices
- *In vivo* 2-photon calcium imaging and pupillometry
- Perfusions and immunolabeling
- Rabies-virus (RV) based retrograde monosynaptic tracing
- Data analyses

● QUANTIFICATION AND STATISTICAL ANALYSIS

## SUPPLEMENTAL INFORMATION

Supplemental information can be found online at https://doi.org/10.1016/j.neuron.2021.05.001.

## ACKNOWLEDGMENTS

We thank all the members of the Spiegel lab for comments and discussions; Shakked Ganor for assistance with animal husbandry; and Drs. Jackie Schiller (Technion, Haifa, Israel), Michal Rivlin, and Amos Arieli (Weizmann Institute of Science, Rehovot, Israel) for critical reading of the manuscript. We also thank Dr. Michal Rivlin for her help with establishing visual stimulation protocols. This work was supported by a Minna James Heineman grant (712566-01 to I.S.), an Israel Science Foundation (ISF) Israeli Centers for Research Excellence (I-CORE) grant (1916/12 to I.S.), a Deutsche Forschungsgemeinschaft (DFG)-Sonderforschungsbereiche (SFB) grant (1089 to I.L.), an ISF grant (1539/17 to I.L.), and a Minerva Foundation grant (to I.L.). I.S. is the incumbent of the Friends and Linda and Richard Price Career Development Chair and a scholar in the Zuckerman STEM leadership program.

## AUTHOR CONTRIBUTIONS

K.C.-K.M. and I.S. initiated and conceived the project. Experiments and analyses were performed by K.C.-K.M. except as follows: all *ex vivo* recordings in acute slices were done by E.T.; rabies-tracing experiments were done by D.K., who also prepared key viral reagents and made essential contributions to 2P imaging; FISH in Figure S1 was done by D.A.; S.S. helped with 2P imaging experiments and their analyses; E.Z. cloned and tested the pAAV-hSyn-Flex-mRuby3 construct; M.S. and I.L. helped with initial 2P imaging and pupillometry experiments and with custom-written software to analyze these experiments (I.L. also helped with analyzing *in vivo* electrophysiology experiments); and G.T. and A.M. helped with establishing and quantifying the rabies-tracing experiments. I.S. supervised the project and acquired funding. K.C.-K.M. and I.S. wrote the manuscript with input and comments from all authors.

## DECLARATION OF INTERESTS

The authors declare no competing interests.

Received: April 6, 2020
Revised: January 28, 2021
Accepted: April 29, 2021
Published: May 25, 2021

## REFERENCES

Abs, E., Poorthuis, R.B., Apelblat, D., Muhammad, K., Pardi, M.B., Enke, L., Kushinsky, D., Pu, D.-L., Eizinger, M.F., Conzelmann, K.-K., et al. (2018). Learning-related plasticity in dendrite-targeting layer 1 interneurons. Neuron *100*, 684–699.e6.

Adesnik, H., Bruns, W., Taniguchi, H., Huang, Z.J., and Scanziani, M. (2012). A neural circuit for spatial summation in visual cortex. Nature *490*, 226–231.

Adler, A., Zhao, R., Shin, M.E., Yasuda, R., and Gan, W.-B. (2019). Somatostatin-expressing interneurons enable and maintain learning-dependent sequential activation of pyramidal neurons. Neuron *102*, 202–216.e7.

Alitto, H.J., and Dan, Y. (2013). Cell-type-specific modulation of neocortical activity by basal forebrain input. Front. Syst. Neurosci. *6*, 79.

Anastasiades, P.G., Collins, D.P., and Carter, A.G. (2021). Mediodorsal and ventromedial thalamus engage distinct L1 circuits in the prefrontal cortex. Neuron *109*, 314–330.e4.

Atallah, B.V., Bruns, W., Carandini, M., and Scanziani, M. (2012). Parvalbumin-expressing interneurons linearly transform cortical responses to visual stimuli. Neuron *73*, 159–170.

Ayzenshtat, I., Karnani, M.M., Jackson, J., and Yuste, R. (2016). Cortical control of spatial resolution by VIP+ interneurons. J. Neurosci. *36*, 11498–11509.

Bar-Ilan, L., Gidon, A., and Segev, I. (2013). The role of dendritic inhibition in shaping the plasticity of excitatory synapses. Front. Neural Circuits *6*, 118.

Brombas, A., Fletcher, L.N., and Williams, S.R. (2014). Activity-dependent modulation of layer 1 inhibitory neocortical circuits by acetylcholine. J. Neurosci. *34*, 1932–1941.

Cadwell, C.R., Palasantza, A., Jiang, X., Berens, P., Deng, Q., Yilmaz, M., Reimer, J., Shen, S., Bethge, M., Tolias, K.F., et al. (2016). Electrophysiological, transcriptomic and morphologic profiling of single neurons using Patch-seq. Nat. Biotechnol. *34*, 199–203.

Carandini, M., and Heeger, D.J. (1994). Summation and division by neurons in primate visual cortex. Science *264*, 1333–1336.

Cauller, L. (1995). Layer I of primary sensory neocortex: where top-down converges upon bottom-up. Behav. Brain Res. *71*, 163–170.

Chen, S.X., Kim, A.N., Peters, A.J., and Komiyama, T. (2015). Subtype-specific plasticity of inhibitory circuits in motor cortex during motor learning. Nat. Neurosci. *18*, 1109–1115.

Chen, T.-W., Wardill, T.J., Sun, Y., Pulver, S.R., Renninger, S.L., Baohan, A., Schreiter, E.R., Kerr, R.A., Orger, M.B., Jayaraman, V., et al. (2013). Ultrasensitive fluorescent proteins for imaging neuronal activity. Nature *499*, 295–300.

Cohen-Kashi Malina, K., Mohar, B., Rappaport, A.N., and Lampl, I. (2016). Local and thalamic origins of correlated ongoing and sensory-evoked cortical activities. Nat. Commun. *7*, 12740.

Cruz-Martín, A., El-Danaf, R.N., Osakada, F., Sriram, B., Dhande, O.S., Nguyen, P.L., Callaway, E.M., Ghosh, A., and Huberman, A.D. (2014). A dedicated circuit links direction-selective retinal ganglion cells to the primary visual cortex. Nature *507*, 358–361.

Dipoppa, M., Ranson, A., Krumin, M., Pachitariu, M., Carandini, M., and Harris, K.D. (2018). Vision and locomotion shape the interactions between neuron types in mouse visual cortex. Neuron *98*, 602–615.e8.

Fan, L.Z., Kheifets, S., Böhm, U.L., Wu, H., Piatkevich, K.D., Xie, M.E., Parot, V., Ha, Y., Evans, K.E., Boyden, E.S., et al. (2020). All-Optical Electrophysiology Reveals the Role of Lateral Inhibition in Sensory Processing in Cortical Layer 1. Cell *180*, 521–535.e18.

Fang, Q., Chou, X.-L., Peng, B., Zhong, W., Zhang, L.I., and Tao, H.W. (2020). A differential circuit via retino-colliculo-pulvinar pathway enhances feature selectivity in visual cortex through surround suppression. Neuron *105*, 355–369.e6.

Fenno, L.E., Mattis, J., Ramakrishnan, C., Hyun, M., Lee, S.Y., He, M., Tucciarone, J., Selimbeyoglu, A., Berndt, A., Grosenick, L., et al. (2014). Targeting cells with single vectors using multiple-feature Boolean logic. Nat. Methods *11*, 763–772.

Ferguson, K.A., and Cardin, J.A. (2020). Mechanisms underlying gain modulation in the cortex. Nat. Rev. Neurosci. *21*, 80–92.

Fishell, G., and Kepecs, A. (2020). Interneuron types as attractors and controllers. Annu. Rev. Neurosci. *43*, 1–30.

Fu, Y., Tucciarone, J.M., Espinosa, J.S., Sheng, N., Darcy, D.P., Nicoll, R.A., Huang, Z.J., and Stryker, M.P. (2014). A cortical circuit for gain control by behavioral state. Cell *156*, 1139–1152.

Fürth, D., Vaissière, T., Tzortzi, O., Xuan, Y., Märtin, A., Lazaridis, I., Spigolon, G., Fisone, G., Tomer, R., Deisseroth, K., et al. (2018). An interactive framework for whole-brain maps at cellular resolution. Nat. Neurosci. *21*, 139–149.

Hu, F., Kamigaki, T., Zhang, Z., Zhang, S., Dan, U., and Dan, Y. (2019). Prefrontal corticotectal neurons enhance visual processing through the superior colliculus and pulvinar thalamus. Neuron *104*, 1141–1152.e4.

Ibrahim, L.A., Mesik, L., Ji, X.-Y., Fang, Q., Li, H.-F., Li, Y.-T., Zingg, B., Zhang, L.I., and Tao, H.W. (2016). Cross-modality sharpening of visual cortical processing through layer-1-mediated inhibition and disinhibition. Neuron *89*, 1031–1045.

Isaacson, J.S., and Scanziani, M. (2011). How inhibition shapes cortical activity. Neuron *72*, 231–243.

Jiang, X., Wang, G., Lee, A.J., Stornetta, R.L., and Zhu, J.J. (2013). The organization of two new cortical interneuronal circuits. Nat. Neurosci. *16*, 210–218.

Jiang, X., Shen, S., Cadwell, C.R., Berens, P., Sinz, F., Ecker, A.S., Patel, S., and Tolias, A.S. (2015). Principles of connectivity among morphologically defined cell types in adult neocortex. Science *350*, aac9462.

Kim, E.J., Jacobs, M.W., Ito-Cole, T., and Callaway, E.M. (2016). Improved monosynaptic neural circuit tracing using engineered rabies virus glycoproteins. Cell Rep. *15*, 692–699.

Klapoetke, N.C., Murata, Y., Kim, S.S., Pulver, S.R., Birdsey-Benson, A., Cho, Y.K., Morimoto, T.K., Chuong, A.S., Carpenter, E.J., Tian, Z., et al. (2014). Independent optical excitation of distinct neural populations. Nat. Methods *11*, 338–346.

Krashes, M.J., Koda, S., Ye, C., Rogan, S.C., Adams, A.C., Cusher, D.S., Maratos-Flier, E., Roth, B.L., and Lowell, B.B. (2011). Rapid, reversible activation of AgRP neurons drives feeding behavior in mice. J. Clin. Invest. *121*, 1424–1428.

Larkum, M.E., Senn, W., and Lüscher, H.-R. (2004). Top-down dendritic input increases the gain of layer 5 pyramidal neurons. Cereb. Cortex *14*, 1059–1070.

Lee, S.-H., Kwan, A.C., Zhang, S., Phoumthipphavong, V., Flannery, J.G., Masmanidis, S.C., Taniguchi, H., Huang, Z.J., Zhang, F., Boyden, E.S., et al. (2012). Activation of specific interneurons improves V1 feature selectivity and visual perception. Nature *488*, 379–383.

Leinweber, M., Ward, D.R., Sobczak, J.M., Attinger, A., and Keller, G.B. (2017). A sensorimotor circuit in mouse cortex for visual flow predictions. Neuron *95*, 59, 1420–1432.

Letzkus, J.J., Wolff, S.B.E., Meyer, E.M.M., Tovote, P., Courtin, J., Herry, C., and Lüthi, A. (2011). A disinhibitory microcircuit for associative fear learning in the auditory cortex. Nature *480*, 331–335.

Lovett-Barron, M., Kaifosh, P., Kheirbek, M.A., Danielson, N., Zaremba, J.D., Reardon, T.R., Turi, G.F., Hen, R., Zemelman, B.V., and Losonczy, A. (2014). Dendritic inhibition in the hippocampus supports fear learning. Science *343*, 857–863.

Mahn, M., Gibor, L., Patil, P., Cohen-Kashi Malina, K., Oring, S., Printz, Y., Levy, R., Lampl, I., and Yizhar, O. (2018). High-efficiency optogenetic silencing with soma-targeted anion-conducting channelrhodopsins. Nat. Commun. *9*, 4125.

Marvin, J.S., Shimoda, Y., Magloire, V., Leite, M., Kawashima, T., Jensen, T.P., Kolb, I., Knott, E.L., Novak, O., Podgorski, K., et al. (2019). A genetically encoded fluorescent sensor for in vivo imaging of GABA. Nat. Methods *16*, 763–770.

McGinley, M.J., David, S.V., and McCormick, D.A. (2015). Cortical membrane potential signature of optimal states for sensory signal detection. Neuron *87*, 179–192.

Meir, I., Katz, Y., and Lampl, I. (2018). Membrane potential correlates of network decorrelation and improved SNR by cholinergic activation in the somatosensory cortex. J. Neurosci. *38*, 10692–10708.

Millman, D.J., Ocker, G.K., Caldejon, S., Kato, I., Larkin, J.D., Lee, E.K., Luviano, J., Nayan, C., Nguyen, T.V., North, K., et al. (2020). VIP interneurons in mouse primary visual cortex selectively enhance responses to weak but specific stimuli. eLife *9*, e55130.

Naskar, S., Qi, J., Pereira, F., Gerfen, C.R., and Lee, S. (2021). Cell-type-specific recruitment of GABAergic interneurons in the primary somatosensory cortex by long-range inputs. Cell Rep. *34*, 108774.

Neske, G.T., Nestvogel, D., Steffan, P.J., and McCormick, D.A. (2019). Distinct waking states for strong evoked responses in primary visual cortex and optimal visual detection performance. J. Neurosci. *39*, 10044–10059.

Olsen, S.R., Bortone, D.S., Adesnik, H., and Scanziani, M. (2012). Gain control by layer six in cortical circuits of vision. Nature *483*, 47–52.

Overstreet-Wadiche, L., and McBain, C.J. (2015). Neurogliaform cells in cortical circuits. Nat. Rev. Neurosci. *16*, 458–468.

Pachitariu, M., Stringer, C., Dipoppa, M., Schröder, S., Federico Rossi, L., Dalgleish, H., Carandini, M., and Harris, K.D. (2017). Suite2p: beyond 10,000 neurons with standard two-photon microscopy. bioRxiv. https://doi.org/10.1101/061507.

Pakan, J.M., Lowe, S.C., Dylda, E., Keemink, S.W., Currie, S.P., Coutts, C.A., and Rochefort, N.L. (2016). Behavioral-state modulation of inhibition is context-dependent and cell type specific in mouse visual cortex. eLife *5*, e14985.

Palmer, L.M., Schulz, J.M., Murphy, S.C., Ledergerber, D., Murayama, M., and Larkum, M.E. (2012). The cellular basis of GABA(B)-mediated interhemispheric inhibition. Science *335*, 989–993.

Pfeffer, C.K., Xue, M., He, M., Huang, Z.J., and Scanziani, M. (2013). Inhibition of inhibition in visual cortex: the logic of connections between molecularly distinct interneurons. Nat. Neurosci. *16*, 1068–1076.

Phillips, E.A., and Hasenstaub, A.R. (2016). Asymmetric effects of activating and inactivating cortical interneurons. eLife *5*, e18383.

Pinto, L., Goard, M.J., Estandian, D., Xu, M., Kwan, A.C., Lee, S.-H., Harrison, T.C., Feng, G., and Dan, Y. (2013). Fast modulation of visual perception by basal forebrain cholinergic neurons. Nat. Neurosci. *16*, 1857–1863.

Reimer, J., Froudarakis, E., Cadwell, C.R., Yatsenko, D., Denfield, G.H., and Tolias, A.S. (2014). Pupil fluctuations track fast switching of cortical states during quiet wakefulness. Neuron *84*, 355–362.

Roth, M.M., Dahmen, J.C., Muir, D.R., Imhof, F., Martini, F.J., and Hofer, S.B. (2016). Thalamic nuclei convey diverse contextual information to layer 1 of visual cortex. Nat. Neurosci. *19*, 299–307.

Scala, F., Kobak, D., Shan, S., Bernaerts, Y., Laturnus, S., Cadwell, C.R., Hartmanis, L., Froudarakis, E., Castro, J.R., Tan, Z.H., et al. (2019). Layer 4 of mouse neocortex differs in cell types and circuit organization between sensory areas. Nat. Commun. *10*, 4174.

Schneider, D.M., Nelson, A., and Mooney, R. (2014). A synaptic and circuit basis for corollary discharge in the auditory cortex. Nature *513*, 189–194.

Schuman, B., Machold, R.P., Hashikawa, Y., Fuzik, J., Fishell, G.J., and Rudy, B. (2019). Four unique interneuron populations reside in neocortical layer 1. J. Neurosci. *39*, 125–139.

Senzai, Y., Fernandez-Ruiz, A., and Buzsáki, G. (2019). Layer-specific physiological features and interlaminar interactions in the primary visual cortex of the mouse. Neuron *101*, 500–513.e5.

Shlosberg, D., Amitai, Y., and Azouz, R. (2006). Time-dependent, layer-specific modulation of sensory responses mediated by neocortical layer 1. J. Neurophysiol. *96*, 3170–3182.

Tamás, G., Lorincz, A., Simon, A., and Szabadics, J. (2003). Identified sources and targets of slow inhibition in the neocortex. Science *299*, 1902–1905.

Tasaka, G.-I., Feigin, L., Maor, I., Groysman, M., DeNardo, L.A., Schiavo, J.K., Froemke, R.C., Luo, L., and Mizrahi, A. (2020). The temporal association cortex plays a key role in auditory-driven maternal plasticity. Neuron *107*, 566–579.e7.

Tasic, B., Menon, V., Nguyen, T.N., Kim, T.-K., Jarsky, T., Yao, Z., Levi, B., Gray, L.T., Sorensen, S.A., Dolbeare, T., et al. (2016). Adult mouse cortical

cell taxonomy revealed by single cell transcriptomics. Nat. Neurosci. *19*, 335–346.

Tremblay, R., Lee, S., and Rudy, B. (2016). GABAergic interneurons in the neocortex: from cellular properties to circuits. Neuron *91*, 260–292.

Vinck, M., Batista-Brito, R., Knoblich, U., and Cardin, J.A. (2015). Arousal and locomotion make distinct contributions to cortical activity patterns and visual encoding. Neuron *86*, 740–754.

Walker, F., Möck, M., Feyerabend, M., Guy, J., Wagener, R.J., Schubert, D., Staiger, J.F., and Witte, M. (2016). Parvalbumin- and vasoactive intestinal polypeptide-expressing neocortical interneurons impose differential inhibition on Martinotti cells. Nat. Commun. *7*, 13664.

Wall, N.R., De La Parra, M., Sorokin, J.M., Taniguchi, H., Huang, Z.J., and Callaway, E.M. (2016). Brain-wide maps of synaptic input to cortical interneurons. J. Neurosci. *36*, 4000–4009.

Watabe-Uchida, M., Zhu, L., Ogawa, S.K., Vamanrao, A., and Uchida, N. (2012). Whole-brain mapping of direct inputs to midbrain dopamine neurons. Neuron *74*, 858–873.

Wickersham, I.R., Lyon, D.C., Barnard, R.J.O., Mori, T., Finke, S., Conzelmann, K.-K., Young, J.A.T., and Callaway, E.M. (2007). Monosynaptic restriction of transsynaptic tracing from single, genetically targeted neurons. Neuron *53*, 639–647.

Wilson, N.R., Runyan, C.A., Wang, F.L., and Sur, M. (2012). Division and subtraction by distinct cortical inhibitory networks in vivo. Nature *488*, 343–348.

Zhang, F., Wang, L.-P., Boyden, E.S., and Deisseroth, K. (2006). Channelrhodopsin-2 and optical control of excitable cells. Nat. Methods *3*, 785–792.

Zhang, S., Xu, M., Kamigaki, T., Hoang Do, J.P., Chang, W.-C., Jenvay, S., Miyamichi, K., Luo, L., and Dan, Y. (2014). Selective attention. Long-range and local circuits for top-down modulation of visual cortex processing. Science *345*, 660–665.

Zolotukhin, S., Byrne, B.J., Mason, E., Zolotukhin, I., Potter, M., Chesnut, K., Summerford, C., Samulski, R.J., and Muzyczka, N. (1999). Recombinant adeno-associated virus purification using novel methods improves infectious titer and yield. Gene Ther. *6*, 973–985.

## STAR★METHODS

### KEY RESOURCES TABLE

| REAGENT or RESOURCE | SOURCE | IDENTIFIER |
|---|---|---|
| **Antibodies** | | |
| Chicken-anti-GFP (diluted 1:1000) | Thermofisher | Cat# A10262; RRID: AB_2534023 |
| Goat-anti-chicken Alexa 488 (diluted 1:1000) | Thermofisher | Cat# A-11039; RRID: AB_2534096 |
| **Bacterial and virus strains** | | |
| AAV.Syn.Flex.GCaMP6s.WPRE.SV40 (AAV1) | Chen et al., 2013 | RRID: Addgene_100845 |
| AAV-hSyn-Flex-rc[Chronos-GFP] (AAV9) | Klapoetke et al., 2014 | RRID: Addgene_62722 |
| AAV-hSyn-hChR2(H134R)-mCherry (AAV9) | Gift from Karl Deisseroth | RRID: Addgene_26976 |
| AAV-hSyn-DIO-hM4D(Gi)-mCherry (AAV8) | Krashes et al., 2011 | RRID: Addgene_44362 |
| AAV-Ef1a-fDIO-GCaMP6s (pDJ) | Gift from Rylan Larsen | RRID: Addgene_105714 |
| AAV-hSyn-Flex-mRuby3-2A (pDJ) | Spiegel Lab | N/A |
| AAV-Ef1a-fDIO-rc[Chronos-eGFP]-WPRE (pDJ) | Spiegel Lab | N/A |
| AAV-Ef1a-fDIO-EYFP-WPRE (pDJ) | Fenno et al., 2014 | RRID: Addgene_55641 |
| AAV-CaMKII-jGCaMP7f-WPRE (pDJ) | Spiegel Lab | N/A |
| AAV-EF1a-FLEX-TVA-mCherry (pDJ) | Watabe-Uchida et al., 2012 | RRID: Addgene_38044 |
| AAV-Ef1a-DIO-oG-WPRE-hGh (pDJ) | Kim et al., 2016 | RRID: Addgene_74290 |
| EnvA-pseudotyped, G-deleted Rabies-eGFP | Tasaka et al., 2020 | N/A |
| **Chemicals, peptides, and recombinant proteins** | | |
| Manual Assay RNAscope Mm-Ndnf-C1 | ACD Bio | Mm-Ndnf-C1 |
| Manual Assay RNAscope Mm-Pvalb-C2 | ACD Bio | Mm-Pvalb-C2 |
| Manual Assay RNAscope Mm-Sst-C2 | ACD Bio | Mm-Sst-C2 |
| Manual Assay RNAscope Mm- Vip-C2 | ACD Bio | Mm- Vip-C2 |
| Manual Assay RNAscope Mm-Reln-C2 | ACD Bio | Mm-Reln-C2 |
| Manual Assay RNAscope Mm-Npy-C2 | ACD Bio | Mm-Npy-C2 |
| Manual Assay RNAscope Mm-Calb-C2 | ACD Bio | Mm-Calb-C2 |
| Manual Assay RNAscope Mm-Nos-C2 | ACD Bio | Mm-Nos-C2 |
| Manual Assay RNAscope Mm-Gad1-C3 | ACD Bio | Mm- Gad1-C3 |
| **Critical commercial assays** | | |
| RNAscope Multiplex Fluorescent Reagent Kit | ACD Bio | 320850 |
| **Experimental models: Organisms/strains** | | |
| Mouse: C57BL/6J | Envigo (Israel) | Order code 057 |
| Mouse: Ndnf-IRES-CreERT2 | The Jackson Laboratory | Cat# JAX:034875; RRID: IMSR_JAX:034875 |
| Mouse: Ndnf-IRES-FlpO | The Jackson Laboratory | Cat# JAX:034876; RRID: IMSR_JAX:034876 |
| Mouse: Sst-IRES-FlpO | The Jackson Laboratory | Cat# JAX:031629; RRID: IMSR_JAX:031629 |
| Mouse: Pv-IRES-Cre | The Jackson Laboratory | Cat# JAX:008069; RRID: IMSR_JAX:008069 |
| **Recombinant DNA** | | |
| pAAV-hSyn-Flex-mRuby3-2A | Spiegel Lab | N/A |
| pAAV-Ef1a-fDIO-rc[Chronos-eGFP]-WPRE | Spiegel Lab | N/A |
| pAAV-CaMKII-jGCaMP7f-WPRE | Spiegel Lab | N/A |
| **Software and algorithms** | | |
| MATLAB | MathWorks | N/A |
| pClamp | Molecular Devices | N/A |
| LabVIEW | LabVIEW | N/A |
| Imaris | BitPlane | N/A |
| WholeBrain | Fürth et al., 2018 | N/A |

## RESOURCE AVAILABILITY

### Lead contact

Further information and requests for resources and reagent should be directed to and will be fulfilled upon reasonable request by the Lead Contact Ivo Spiegel (ivo.spiegel@weizmann.ac.il).

### Materials availability

With the exception of the newly sub-cloned AAV plasmids pAAV-hSyn-Flex-mRuby3-2A, pAAV-Ef1a-fDIO-rc[Chronos-eGFP]-WPRE and pAAV-CaMKII-jGCaMP7f-WPRE, no new reagents were created in this study. These newly created plasmids are available upon request from the Lead Contact until they will be deposited at Addgene.

### Data and code availability

The datasets and the scripts used in study are available from the Lead Contact upon reasonable request.

## EXPERIMENTAL MODEL AND SUBJECT DETAILS

### Mice

All procedures involving animals were reviewed and approved by the Weizmann Institutional Animals Care Committee. Recordings were made from young adult mice of either sex, housed up to five animals per cage in a 12/12 hours reverse dark/light cycle. All mice used in this study were either C57Bl6/J WT or heterozygous for the indicated genotypes (i.e., for Ndnf-IRES-CreERT; Ndnf-IRES-FlpO; Sst-IRES-FlpO; Pv-IRES-Cre; Ndnf-IRES-CreERT:: Sst-IRES-FlpO; Ndnf-IRES-FlpO:: Pv-IRES-Cre).

## METHOD DETAILS

### Fluorescent *in situ* hybridization (FISH)

FISH and subsequent analyses were done with the RNAscope system (Advanced Cell Diagnostic) on PFA-fixed sections of 8-week old fresh-frozen mouse brains, exactly as previously described (Abs et al., 2018). All probes and reagents were purchased from Advanced Cell Diagnostic.

### AAV stocks

AAV constructs were purchased either in packaged form the respective source or as plasmids from Addgene and then packaged in pDJ essentially as described (Zolotukhin et al., 1999). The plasmids for AAV-hSyn-Flex-mRuby3-2A, AAV-Ef1a-fDIO-rc[Chronos-eGFP]-WPRE and AAV-CaMKII-jGCaMP7f-WPRE were generated by sub-cloning the respective inserts into suitable AAV backbones using standard cloning methods; AAVs for these plasmids were packaged in pDJ.

### Viral injections and cranial window implantations

Mice were anesthetized with isoflurane at an initial concentration of 4% and a maintenance level of 1.5%–2%. The mice were fixed in a stereotaxic apparatus (Kopf Instruments, model 942) and ophthalmic ointment (Duratears) was applied to the eyes. Body temperature was kept at 37°C with a heating blanket (RWD Life science). Before the surgical procedure, local anesthesia (2% Lidocaine) was injected under the scalp and the skin was scrubbed with 70% ethanol and betadine. A craniotomy was made above the left visual cortex (centered 2.7 mm posterior and 2.5 mm lateral to the bregma). For mapping experiment, the craniotomy was made above the auditory cortex (2.46 mm posterior and 4.5 mm lateral to the bregma) or the anterior cingulate cortex (1 mm anterior and 0.3 mm lateral to the bregma). 2-3 injections of 300 nL of virus were made using a beveled glass micropipette at a depth of 300 μM with a microsyringe pump (UMP3T-2, WPI). After the injection, the skin of the mice intended for electrophysiology studies was sealed with VetBond (3M). For imaging study, a 3 mm craniotomy above the visual cortex was made and following the viral injection, a cover glass was glued to the skull using VetBond (3M) and a custom-made head-post was glued to the skull (Krazy glue). Following surgery the animals were administered with analgesic (0.1 mg/kg of buprenorphine and 5mg/kg of Carprofen). Expression of all AAVs was induced 1 week post intractortical AAV-injection by intraperitoneal injection of tamoxifen (200-250μl, 10mg/ml, dissolved in 90% corn oil and 10% ethanol) on 3 consecutive days.

### Preparation of animals for *in vivo* electrophysiological recordings

#### *Anaesthetized animals*

Mice were anesthetized by intraperitoneal injection of 1 g/kg of urethane and 10 mg/kg of chlorprothixene. A thin layer of silicon oil was applied to the eyes to prevent drying. A craniotomy (~1 mm in diameter) was made above the monocular zone of the visual cortex. The craniotomy was constantly washed with artificial cerebrospinal fluid (ACSF) containing (in mM): 123 NaCl, 26 $NaHCO_3$, 11 glucose, 3 KCl, 1.25 $NaH_2PO_4$, 1 $MgCl_2$ and 2 $CaCl_2$. Body temperature was kept at 37°C using a heating blanket.

### *Awake animals*

The preparation of awake mice was done as previously described (Cohen-Kashi Malina et al., 2016). Briefly, the mouse was anesthetized with isoflurane and a custom-made headpost was glued to the exposed skull. Following a recovery period of at least 3 days, the mouse was anesthetized and a craniotomy was made and then covered with spongostan absorbed with ASCF and silicon rubber (Smooth-On). Following a recovery period of 2 hours, the animal was returned to the set and head-fixed for the electrophysiological recordings.

### *In vivo* patch-clamp electrophysiology in the cortex

*In vivo* recordings were performed at least 3 weeks after tamoxifen administration. Borosilicate micropipettes were pulled to produce electrodes with a resistance of 7–10 MΩ and filled with an intracellular solution containing the following (in mM): 135 K-gluconate, 4 KCl, 10 HEPES, 10 phosphocreatine, 4 MgATP, 0.3 NaGTP, and 2 Na2-ATP (310 mOsm). Intracellular and extracellular signals were acquired using an Axoclamp-700B amplifier (Molecular Devices) and low passed at 3 kHz before being digitized at 20 kHz (Digidata 1550, Molecular Devices). Recording depth ranged between 150 and 800 μm. Cells at the depth of 150-350 μm were classified as L2/3, cells at the depth of 350-550 μm were classified as L4 and cells at the depth of 550-800 μm were classified as L5. Cell-attached recordings were obtained after a seal of a few hundred MΩ was reached. Intracellular current clamp recordings were obtained after successful breach of a giga-seal.

### Visual stimulation

Visual stimuli were created using MATLAB with Psychophysics Toolbox (http://psychtoolbox.org/) and presented on a gamma corrected LCD screen. The monitor was positioned 15cm (electrophysiology) or 20cm (imaging) from the contralateral eye of the recording hemisphere and it covered 100° horizontally and 85° vertically of the mouse visual field. Sinusoidal drifting bar gratings with spatial frequency of 0.04 cycles per degree, temporal frequency of 2 Hz and of 100% contrast were displayed in 8 direction evenly spaced in a pseudorandom order. For imaging experiments, we presented drifting sinusoidal gratings with varying contrast (10, 25, 40, 65 and 100%) at a constant spatial frequency (0.04 cpd) and temporal frequency (2 Hz) to test contrast dependency, and in varying spatial frequencies (0.01, 0.04, 0.1, 0.15 and 0.3 cpd) at a constant contrast (100%) and temporal frequency (2 Hz). Prior to the size tuning experiment we did receptive field mapping by presenting circular patches of drifting sinusoidal gratings (set to 25 degrees) spacing on 3 by 4 grid. Stimuli were presented for 1sec at the four cardinals directions with interstimulus intervals of 4 s in which a gray screen of mean luminance was presented. For size tuning experiments the screen was placed at the center of the receptive field of the majority of the imaged neurons and patches of drifting sinusoidal gratings at 5 different sizes (5, 10, 35, 60 and 80 degrees) at constant contrast (100%), spatial frequency (0.04 cpd) and temporal frequency (2Hz) were presented. Stimulus presentation duration was 2 s and interstimulus intervals were either 5 s (imaging) or 8 s (electrophysiology) in which a gray screen of mean luminance was displayed. A minimum of 6 (electrophysiology) up to 15 repetitions (imaging and electrophysiology) were presented per stimulus.

For the chemogenetic experiments, drifting sinusoidal gratings at evenly spaced 8 directions with 50 repetitions were presented for 1 s with 3 s of interstimulus intervals in which gray screen of mean luminance was displayed.

During $Ca^{2+}$ imaging session when ongoing activity was recorded and no visual stimuli were presented, a gray screen of mean luminance was displayed.

### Optogenetic stimulation

In *in vivo* optogenetic experiments, L1 NDNF IN were activated or silenced in interleaved trials of visual stimulation by turning on an LED (Prizmatix, 470nm, optical fiber diameter of 200 μm, 1mW) 50 ms before the start and then throughout the visual stimulus. To prevent the LED light from leaking to the eyes, we shielded the LED with black tape. We found no effect of LED activation on visually evoked responses in control mice (Figure S3F).

In the *in vitro* mapping experiment, optogenetic stimulation was performed using whole field illumination (470nM, Lumincore SPECTRA X light engine, through Olympus 40x objective, 4.1mW) delivered through the microscope illumination path.

### Chemogenetic silencing of L1 NDNF INs

To validate the suppression of L1 NDNF INs by the chemogenetic manipulation we co-expressed the Cre-dependent inhibitory DREADD hM4Di and Cre-dependent Chronos-GFP (ratio of 1:1 ) in L1 NDNF INs and recorded evoked IPSCs in L2/3 pyramidal neurons prior and after bath application of Compound 21 (final concentration of 5 μM Sigma-Aldrich,SML2392) or vehicle.

To suppress the activity of L1 NDNF INs and measured the evoked-responses of L2/3 excitatory neurons *in vivo*, we co injected the Cre-dependent inhibitory DREADD hM4Di and CaMKII-GCaMP7f (ratio of 4:1) in NDNF-Cre-ERT2 mice. Following 3 weeks of expression, evoked responses of L2/3 excitatory neurons were recorded prior and 30 minutes after I.P injection of Compound 21 (3mg/kg) or vehicle.

### Patch-clamp electrophysiology in acute visual cortex slices

Acute brain slices from the visual cortex of P60 mice were prepared as previously described (Abs et al., 2018; Mahn et al., 2018). Whole-cell patch clamp recordings were performed using Scientifica slice scope. Borosilicate micropipettes were pulled to produce

electrodes with a resistance of 3–6 MΩ and filled with patch solution (in mM): 135 $CsMeSO_4$, 10 phosphocreatine, 10 HEPES, 0.3 $Na_3GTP$, 1 MgATP, 3 QX-314 and 4TEA-Cl; 310 mOsm. Prior to the experiment, CF 594 hydrazide (Sigma-Aldrich, SCJ4600029) was added into the internal solution (1 μm final concentration) to visualize the recorded cells under the slice microscope and verify that they were indeed pyramidal neurons, based on the morphology, and to estimate the relative distance of the soma from the pia. Voltage-clamp recordings were made using Multiclamp 700B amplifiers (Axon Instruments, CA), low-pass filtered at 3kHz and digitized 20 kHz (Digidata 1550, Molecular Devices). Slices were perfused with carbogenated ACSF and maintained at 32°C. IPSCs or EPSCs were recorded at a 0mV or −70mV holding potential, respectively, and in the presence of TTX (0.5μM) and 4-AP (100μM). Cells were discarded if they had an access resistance larger than 25 MΩ during the recordings.

### *In vivo* 2-photon calcium imaging and pupillometry

2-photon imaging: Imaging was performed at least two weeks after tamoxifen administration using a two-photon microscope with a 12 kHz resonant-galvo scanhead (Bergamo microscope, ThorLabs) at an acquisition rate of 11Hz. Frame size was 512 × 512 pixels. Illumination was provided by a Mai Tai DeepSee laser at 930nM. Pupillometry: During imaging, the mouse's ipsilateral eye was illuminated with an IR-light source (M940L3, Thorlabs) and imaged using a CMOS camera at 33Hz.

For imaging in anesthetized mice, mice were anesthetized by intraperitoneal injection of 1 g/kg of urethane and 10 mg/kg of chlorprothixene. A thin layer of silicon oil was applied to the eyes to prevent drying. Body temperature was kept at 37°C using a heating blanket.

### Perfusions and immunolabeling

Perfusions and immunolabeling were done as previously described (Abs et al., 2018). In brief, mice were anesthetized with 10% ketamine and 1% xylazine in PBS and transcardially perfused with ice cold PBS for five minutes followed by fifteen minutes of cold 4% PFA in PBS. Brains were then dissected, post-fixed for 1 hour at 4°C in 4% PFA, washed three times in cold PBS, and cryoprotected overnight in 20% sucrose in PBS at 4°C. The brains were frozen in Tissue-Tek Cryo-OCT compound (Fisher Scientific) on dry ice and stored at −80°C. Coronal sections (15 μm thick) of visual cortex were cut using a Leica CM1950 cryostat and mounted on SuperFrost Plus glass slides (Fisher Scientific). Chronos-GFP was visualized by immunolabeling against GFP, stGtACR2-fRed was visualized directly via fRed-fluorescence. Immunolabeling for GFP was done by blocking the sections for 1 hour in blocking buffer (PBS with 5% normal goat serum and 0.1% Triton X-100), staining the samples overnight with Chicken-anti-GFP primary antibody (Thermofisher, A10262, diluted 1:1000 in blocking buffer), followed by three washes in PBS and staining with Goat-anti-chicken Alexa 488 secondary antibody (Thermofisher, A11039, diluted 1:1000) and Hoechst counterstain for 45 min at room-temperature. After mounting in FluoromountG (Southern Biotech), the stained sections were imaged on a Zeiss LSM 800 confocal microscope.

### Rabies-virus (RV) based retrograde monosynaptic tracing

Rabies tracing was performed similarly as previously described (Tasaka et al., 2020). Briefly, NDNF-Ires-CreERT2 mice were injected with 250 nL of a 1:1 dilution of AAV-Ef1a-DIO-oG-WPRE-hGh (Addgene plasmid #74290) and AAV-EF1a-FLEX-TVA-mCherry (Addgene plasmid #38044) unilaterally into V1. Mice were allowed to recover for 1 week and were then administered tamoxifen for 3 consecutive days. 2 weeks following tamoxifen administration, mice were injected with GFP expressing EnvA-Pseudotyped RabiesΔG. Following 5 days of RV expression, mice were perfused transcardially for 5 minutes with ice cold PBS followed by 4% PFA in PBS for 15 minutes. Whole brains were extracted, postfixed in 4% PFA for 1 hour, washed with cold PBS, and cryoprotected in 20% sucrose in PBS overnight. Brains were embedded in OCT and sliced into 50μm frozen sections (Cryostat). Sections were then incubated in blocking solution (10% NGS with 0.5% Triton-X in PBS) and then stained with anti-GFP antibody to enhance signal (Biotin anti-GFP (1:200, overnight) followed by 488 Streptavidin (1:1000, for 1 hour)) and imaged using a fluorescent microscope (Slidescanner, Olympus). Cells (GFP = cells that were retrogradely labeled via RV-infection; mCherry = AAV-infected "starter" cells) were semi-automatically registered according to brain region using the WholeBrain software (Fürth et al., 2018). Only mice in which the starter cells were restricted to the visual cortex were included in the quantification/analyses.

### Data analyses

All recordings (electrophysiology and Fluorescent (F) signals derived from 2-photon imaging) were analyzed using custom software written in MATLAB (The MathWorks). Pupil size was analyzed using custom software written in LabView (NI). Unless otherwise noted, all error bars represent mean ± s.e.m. Data in Figures 3D and 3F are presented as MATLAB box-plots.

#### *Analysis of $Ca^{2+}$ 2-photon imaging data*

Raw calcium movies were analyzed using Suite2p (Pachitariu et al., 2017). Neuropil corrected signals were resampled to 0.1, 1 or 5 kHz using a linear interpolation. For cross-correlation measurements, F signals were smoothed with a Savitzky–Golay filter with a first-order polynomial and a window size of 5001 points. Cross-correlation coefficient (CC), at 0 time-lag, of ongoing activity was calculated between all possible pairs per recordings and between each cell and the calculated pupil diameter (see below) for a time window of 15 minute (obtained in a separate imaging session). Shuffle correlations were computed as the correlation between each imaged cell and the inverse signal of the pupil or one of the cells in the cell-to-cell correlation. Visually evoked responses were calculated as the mean ΔF/F during visual stimulus presentation:

$$\Delta F/F = (F - F0)/F0$$

Baseline fluorescence (F0) was calculated as the mean fluorescence of the preceding 1 s. The preferred direction was defined as the direction in which the gratings elicited the largest response. Preferred contrast was determined as the contrast that elicited the largest response at the preferred direction. To determine if a cell was significantly responsive to the drifting grating stimulus, a one-way ANOVA was computed comparing the evoked responses to baseline fluorescence. A neuron was called orientation tuned if it responded significantly different to one of the presented directions as measured by one-way ANOVA. Orientation tuning was measured for all the cells called visually responsive to drifting gratings presented at 100% contrast at 0.04 cpd, using global orientation selectivity index (gOSI):

$$gOSI = \left| \left( \sum R(\theta) \times e^{2i\theta} \right) \Big/ \sum R(\theta) \right|$$

where $R(\theta_k)$ is the response to angle $\theta_k$ (Figure S2C). To generate population average we normalized the responses of each neuron to the maximum response and centered it to 0°. We then averaged the normalized responses of all cells and fitted it using a double Gaussian (see below).

Correlation between pupil diameter and the visually evoked responses in the different cell types was calculated as the relation between the mean evoked response (ΔF/F) of each cell at its preferred direction (at 100% contrast, 0.04 cpd) and the mean pupil diameter measured 1 s after the start of visual stimulation for a total duration of 2 s (1 s in the chemogenetic silencing experiments) so that it matched the duration of the visual stimulus (McGinley et al., 2015; Neske et al., 2019).

#### *Pupil diameter measurement*

Frames were filtered using a median filter and thresholded to low IR light reflectance areas. The resulting regions were then filtered based on circularity and size until only the region corresponding to the pupil remained, as verified manually during each analysis. Consequently an ellipse was fitted to this region by setting its major and minor axes equal to the longer and shorter lines of symmetry of the bounding rectangle. The pupil diameter was estimated as the geometric mean of the major and minor axes.

#### *In vivo electrophysiology*

Recorded neurons were classified as excitatory or fast spiking neuron post hoc based on their peak-to-trough width (Senzai et al., 2019). Visually evoked spikes were calculated as the sum of spikes observed during the period of 70 ms after the start of visual stimulation up to 70 ms after the termination of the stimulus and subtracted by the baseline spiking measured 500ms before visual stimulus presentation. Only visually responsive cells were included in analysis (determined as above). Direction selectivity index (DSI) was calculated as

$$(R_{pref} - R_{null}) / (R_{pref} + R_{null})$$

where $R_{pref}$ is the response to the stimulus that produced the maximum response and $R_{null}$ is the mean response to the opposite direction. Orientation tuning was measured as above. As response values can be negative, especially for non-preferred stimulus conditions, some DSI and gOSI had values greater than 1. All values were used for analysis but for presentation purposes gOSI values greater than 1.6 and DSI values greater than 1.2 were not plotted. Values from anesthetized and awake recordings were pulled together.

To generate population average we normalized the responses of each neuron to the maximum response during LED OFF condition and centered it to 0°. We then averaged the normalized responses of all cells and fitted it using a double Gaussian:

$$R = C + R_{pref} * e^{-(\theta - \theta_{pref})^2 / (2*\sigma^2)} + R_{null} * e^{-(\theta null - \theta pref)^2 / (2*\sigma^2)}$$

Where C is a constant offset. The two Gaussians were forced to peak 180° apart and to have the same width but could have different amplitudes. Preferred orientations were determined using this fit.

Signal to noise ratio (SNR) was calculated as previously described (Meir et al., 2018) for each neuron at its preferred direction as the difference between the evoked response and the inter stimulus time interval divided by the sum of them.

#### *In vitro electrophysiology*

IPSC and EPSC amplitudes were calculated as the difference between peak response and baseline determined as the mean of a time window of 100ms before stimulus onset.

Inhibitory charge (Q) was calculated as the time integral of the IPSCs over the period of LED illumination. Decay time was calculated as the 90%–10% fall time.

## QUANTIFICATION AND STATISTICAL ANALYSIS

The number of experimental recordings and animals used in each experiment is indicated in the figure legends. For *in vitro* recordings we used 2-4 mice per condition. Statistical tests were performed using MATLAB, p values and statistical tests used are indicated in the figure legends.